



UPPSALA  
UNIVERSITET

*Digital Comprehensive Summaries of Uppsala Dissertations  
from the Faculty of Pharmacy 278*

# Advanced Mass Spectrometry Imaging in Neuropharmacology

THEODOSIA VALLIANATOU



ACTA  
UNIVERSITATIS  
UPSALIENSIS  
UPPSALA  
2019

ISSN 1651-6192  
ISBN 978-91-513-0739-8  
urn:nbn:se:uu:diva-392320

Dissertation presented at Uppsala University to be publicly examined in Room B42, Uppsala biomedicinska centrum (BMC) Husargatan 3, Uppsala, Friday, 18 October 2019 at 09:15 for the degree of Doctor of Philosophy (Faculty of Pharmacy). The examination will be conducted in English. Faculty examiner: Associate Professor Nathalie Agar (Harvard Medical School).

### **Abstract**

Vallianatou, T. 2019. *Advanced Mass Spectrometry Imaging in Neuropharmacology. Digital Comprehensive Summaries of Uppsala Dissertations from the Faculty of Pharmacy* 278. 68 pp. Uppsala: Acta Universitatis Upsaliensis. ISBN 978-91-513-0739-8.

Mass spectrometry imaging (MSI) has emerged as a valuable approach for mapping multiple molecular species in sections of diverse tissues. It enables simultaneous detection of numerous compounds (from neurotransmitters to small proteins) in the brain at relatively high lateral resolution (>5  $\mu\text{m}$ ) on a routine basis. Matrix-assisted laser desorption/ionization (MALDI)-MSI and desorption electrospray ionization (DESI)-MSI are the most widely applied MSI techniques in tissue distribution studies. Recent advances in MSI instruments and software allow quantitative analysis of large numbers of compounds with high mass accuracy and high mass resolving power. Thus, in studies this thesis is based upon, MSI technology was used to address several challenging aspects of neuropharmacology. Restricted passage of potentially neuroactive substances into the brain, unpredictable multi-target effects, and the complexity of the central nervous system (CNS) physiology, are major obstacles in the development of efficient drugs. The simultaneous investigation of drugs' delivery to the brain and potential effects on several CNS pathways in specific brain regions is, therefore, highly important. In addition, localization information is required for more comprehensive insights into CNS responses to both pharmaceutical agents and biological processes such as aging.

MSI-based analysis of the transport of two selected drugs into the brain demonstrated effects of efflux membrane proteins on their distributions in the brain. The MDR1 substrate loperamide was found to localize specifically in the choroid plexus, indicating low brain entrance. In addition, MSI uncovered drug-drug interactions at the blood-brain barrier involving MDR1 inhibition. The technology was further used to explore neurochemical alterations induced by aging and acetylcholinesterase inhibition. First, MSI revealed that the cholinergic system's responsivity in the retrosplenial cortex, a post-cingulate cortical area highly involved in cognition, to acetylcholinesterase inhibition significantly declined with age. Subsequently, simultaneous investigation of multiple brain metabolic pathways in specific brain areas with multivariate data analysis techniques demonstrated age-induced alterations in mitochondrial function, lipid signaling, and acetylcholine metabolism. Finally, MSI unveiled age-induced alterations in levels and distributions of the monoaminergic neurotransmitters and their metabolites in particular brain areas such as the ventral pallidum, caudate putamen, hippocampus, and cortical substructures. Age- and region-specific effects of acetylcholinesterase inhibition on the neurotransmitter systems were also detected. In conclusion, the studies provided novel insights into important brain pharmacokinetic and pharmacodynamic phenomena using advanced MSI techniques, as described and discussed in this thesis.

*Keywords:* mass spectrometry imaging, neuropharmacology, blood brain barrier, drug-drug interactions, aging, tacrine

*Theodosia Vallianatou, Department of Pharmaceutical Biosciences, Box 591, Uppsala University, SE-75124 Uppsala, Sweden.*

© Theodosia Vallianatou 2019

ISSN 1651-6192

ISBN 978-91-513-0739-8

urn:nbn:se:uu:diva-392320 (<http://urn.kb.se/resolve?urn=urn:nbn:se:uu:diva-392320>)

*ὁ δὲ ἀνεξέταστος βίος οὐ βιωτὸς ἀνθρώπῳ*

Plato, Socrates Apology



# List of Papers

This thesis is based on the following papers, which are referred to in the text by the corresponding Roman numerals. For convenience, the studies described in Papers I-IV are referred to as Studies I-IV, respectively.

- I **Vallianatou T**, Strittmatter N, Nilsson A, Shariatgorji M, Hamm G, Pereira M, Källback P, Svenningsson P, Karlgren M, Goodwin RJA, André PE (2018) A mass spectrometry imaging approach for investigating how drug-drug interactions influence drug blood-brain barrier permeability. *Neuroimage*, 15:808-816
- II **Vallianatou T**, Shariatgorji M, Nilsson A, Fridjonsdottir E, Källback P, Schintu N, Svenningsson P, André PE (2019) Molecular imaging identifies age-related attenuation of acetylcholine in retrosplenial cortex in response to acetylcholinesterase inhibition. *Neuropsychopharmacology*, doi: 10.1038/s41386-019-0397-5.
- III **Vallianatou T**, Shariatgorji M, Nilsson A, Karlgren M, Hulme H, Fridjonsdottir E, Svenningsson P, André PE. Imaging age-induced perturbations of mitochondrial function, neurotransmission and lipid signaling in specific brain regions. *Submitted*
- IV Fridjonsdottir E\*, **Vallianatou T\***, Shariatgorji M, Nilsson A, Odell LR, Svenningsson P, André PE. Imaging aging effects on the catecholamine, serotonin, and histamine neurotransmitter systems in specific brain regions. *In manuscript*

\*These authors contributed equally

Reprints were made with permission from the respective publishers.

## List of Additional Papers

Nilsson A, Goodwin RJ, Shariatgorji M, Vallianatou T, Webborn PJ, André PE (2015) Mass spectrometry imaging in drug development. *Analytical Chemistry*, 87:1437-1455.

Shariatgorji M, Strittmatter N, Nilsson A, Källback P, Alvarsson A, Zhang X, Vallianatou T, Svenningsson P, Goodwin RJ, Andren PE (2016) Simultaneous imaging of multiple neurotransmitters and neuroactive substances in the brain by desorption electrospray ionization mass spectrometry. *Neuroimage*, 1:129-138

Shariatgorji M, Nilsson A, Fridjonsdottir E, Vallianatou T, Katan L, Sävmarker J, Mantas I, Zhang X, Bezard E, Svenningsson P, Odell L, André PE (2019) Comprehensive mapping of neurotransmitter networks by MALDI-MS imaging. *Nature Methods*, In press

# Contents

Introduction.....	13
Mass Spectrometry Imaging.....	14
Matrix-assisted laser desorption/ionization .....	14
Desorption electrospray ionization .....	15
MSI Instrumentation: Mass Analyzers .....	16
Brain Sample Preparation .....	17
MSI Data Analysis.....	18
Neuroactive molecules in the brain.....	20
Brain pharmacokinetics: drug transport through the brain barriers and distribution in the CNS .....	20
Brain pharmacodynamics: molecular neuropharmacology and major neurotransmitter systems .....	22
Neuroimaging of age-induced alterations.....	24
Aims.....	26
Methods .....	27
Animal experiments .....	27
Tissue processing .....	28
Tissue sectioning .....	28
Quantification of drugs and neurotransmitters .....	28
Preparation of brain tissue sections .....	29
Mass Spectrometry Imaging.....	30
Histological staining of tissue sections .....	31
Imaging data analysis.....	31
Statistical analysis .....	31
Identification of metabolites.....	32
Permeability screening study and <i>in vitro</i> transport experiments .....	32
Results and Discussion .....	34
MSI of MDR1-mediated efflux effects on drug distribution in the brain (Paper I).....	34
The highly permeable compound propranolol was distributed throughout the brain tissue.....	35
Specific localization of loperamide in the choroid plexus as an indicator of limited entry into the brain parenchyma .....	36
MDR1 inhibition-mediated DDIs at the BBB .....	37

Region-specific effects of aging and tacrine-induced AChE inhibition on multiple neurochemical systems (Papers II-IV).....	38
Quantification of ACh brain levels: age-related attenuation in the retrosplenial cortex in response to tacrine (Paper II).....	39
Quantification of tacrine in mouse brain tissue sections: effects of aging on brain distribution (Paper II).....	41
Age-induced metabolic alterations in the CNS (Paper III) .....	42
Effects of aging and AChE inhibition by tacrine on acetylcholine and L-carnitine metabolism .....	43
Age-induced increases in antioxidant and neuroprotective molecules .....	44
Impact of age on brain lipids .....	45
Aging effects on the catecholamine, serotonin, histamine and GABA neurotransmitter systems in the brain (Paper IV).....	47
Conclusions.....	52
Populärvetenskaplig sammanfattning .....	54
Acknowledgements.....	56
References.....	58

# Abbreviations

3-MT	3-methoxytyramine
5-HT	Serotonin
9AA	9-aminoacridine
12-w	12 weeks
14-m	14 months
ABC	ATP-binding cassette
Acb	Nucleus accumbens
ACh	Acetylcholine
AChE	Acetylcholinesterase
AD	Alzheimer's disease
$\alpha$ -GPC	L- $\alpha$ -glycerophosphocholine
Amy	Amygdala
BBB	Blood-brain barrier
BCRP	Breast cancer resistance protein
BCSFB	Blood-cerebrospinal fluid barrier
BNST	Bed nucleus of stria terminalis
CASI	Continuous accumulation of selected ion
Cb	Cerebellum
cc	Corpus callosum
CDP-choline	Cytidine 5'-diphosphate choline
Cg	Cingulate cortex
ChAT	Choline acetyl transferase
CHCA	$\alpha$ -cyano-4-hydroxycinnamic acid
CNS	Central nervous system
COMT	Catechol-O-methyl transferase
CPu	Caudate putamen
CSF	Cerebrospinal fluid
Cx	Cortex
DA	Dopamine
DDI	Drug-drug interaction
DESI	Desorption electrospray ionization

DHB	2,5-dihydroxybenzoic acid
DOPAL	3,4-dihydroxyphenylacetaldehyde
DOPEG	3,4-dihydroxyphenylglycol
DPP-TFB	2,4-diphenyl-pyranylium tetrafluoroborate
ER	Efflux ratio
FMP	Fluoromethyl pyridinium
FTICR	Fourier transform ion cyclotron resonance
GABA	$\gamma$ -aminobutyric acid
H&E	Hematoxylin and eosin
HexCer	Hexosylated ceramide
Hip	Hippocampus
His	Histamine
Hyp	Hypothalamus
i.p.	Intraperitoneal
i.v.	Intravenous
ic	Internal capsule
ITO	Indium tin oxide
LC	Locus coeruleus
LC/MS	Liquid chromatography/mass spectrometry
<i>m/z</i>	Mass-to-charge ratio
MALDI	Matrix-assisted laser desorption/ionization
MAO	Monoaminoxidase
MDCK	Madin-Darby canine kidney II cells
MDR1	Multidrug resistance 1 protein
mbf	Medial forebrain bundle
MOPEG	3-methoxy-4-hydroxyphenylglycol
MS	Mass spectrometry
MS/MS	Tandem mass spectrometry
MSDB	Medial septal nucleus/diagonal band
MSI	Mass spectrometry imaging
MVDA	Multivariate data analysis
Nd:YAG	Neodymium-doped yttrium aluminum garnet
NE	Norepinephrine
OCTN	Organic cation/carnitine transporter
OH-tacrine	Hydroxylated tacrine
PALv	Ventral pallidum
PC	Phosphatidylcholine
PCA	Principal component analysis

PD	Parkinson's disease
PET	Positron emission tomography
PLS-DA	Partial least squares-projection to latent structures-discriminant analysis
RMS	Root mean square
RS	Retrosplenial cortex
SC	Somatosensory cortex
SIMS	Secondary ion mass spectrometry
SNe	Substantia nigra pars compacta
Str	Striatum
TFA	Trifluoroacetic acid
Th	Thalamus
TIC	Total ion count
TOF	Time-of-flight
Tu	Olfactory tubercle
UV	Ultraviolet
VT	Ventral tegmentum



# Introduction

Aging of the global population, and strongly associated increases in numbers of patients suffering from neurological disorders [1], has led to increasing demands for novel neuropharmacological therapies. However, the attrition and failure rates of neuroactive drug development programs are very high, leading to downsizing of many pharmaceutical companies' neuroscience departments [2]. Clearly, therefore, new and more efficient strategies are required to attenuate the progressively increasing impact of neurological diseases on global health.

Pharmacological targeting of the central nervous system (CNS) is not a trivial task due to critical bioavailability and safety aspects [3,4]. The brain tissue has limited accessibility related to the blood-brain barrier (BBB), which often severely restricts drugs' efficacy [4]. Moreover, despite enormous progress and neuropharmacological advances in recent decades, the complexity of the CNS, which consists of numerous interacting neural networks, still limits knowledge of (patho)physiological mechanisms, including crucial cellular senescence processes [2,5]. In addition, as for any therapeutic agents, the toxicity of drugs targeting the CNS is a major concern. Thus, simultaneous investigation of such drugs' delivery to the brain and their potential effects on all potentially influenced CNS pathways, i.e., brain pharmacokinetics and pharmacodynamics, in early stages of drug development is highly important.

The increased prevalence of neurological disorders also raises needs for early detection of biomolecular alterations indicating physiological and pathological states, including senescence, to enable early prognosis and, subsequently, effective treatment [2,5]. Similarly, acquisition of detailed brain tissue localization data for both administered molecules and endogenous compounds is crucial.

A technique that has several major advantages for such applications, and thus has been increasingly applied in neuropharmacology studies to explore distributions of drugs and neurotransmitters in the brain, is mass spectrometry imaging (MSI) [6-9]. It is a direct technique, i.e., it does not require the use of antibodies or labeled markers, it allows thousands of molecules to be simultaneously analyzed at relatively high lateral resolution ( $>5 \mu\text{m}$ ), and it does not require tedious sample preparation and analysis [10]. MSI can, therefore, be a valuable approach for addressing the mentioned critical challenges of neuroscience.

In the studies underlying this thesis, MSI was used to investigate brain pharmacokinetic and pharmacodynamic phenomena and detect age-induced neurochemical alterations. The technique is described in the next paragraphs, which are followed by a detailed description of the current knowledge of, and challenges posed by, addressed aspects of neuropharmacology.

## Mass Spectrometry Imaging

The most widely applied MSI techniques are matrix-assisted laser desorption/ionization (MALDI), desorption electrospray ionization (DESI) and secondary ion mass spectrometry (SIMS) [10]. SIMS-MSI can provide higher lateral resolution (often sub- $\mu\text{m}$ ) than the other methods. However, the ionization involved in SIMS is too harsh for many analytes, limiting its application to elemental and lipid analyses [10]. DESI-MSI requires much less sample preparation than MALDI-MSI, but it offers lower lateral resolution. Both MALDI and DESI-MSI methods have been developed for mapping brain distributions of endogenous metabolites and drugs [11-14]. In addition, brain transport and distributions of pharmaceutical molecules have been investigated by MALDI-MSI [15] as well as brain pharmacokinetics-pharmacodynamics [16]. DESI-MSI has often demonstrated higher sensitivity towards certain analytes than MALDI-MSI, and has been applied in increasing numbers of studies on CNS distributions of small molecules [9,14,17]. In the studies this thesis is based upon, both MALDI- and DESI-based approaches were applied, hence the techniques are further described below.

### Matrix-assisted laser desorption/ionization

As an ionization technique, MALDI was initially introduced in 1988 [18,19] and was used for analysis of diverse large, nonvolatile molecules, such as proteins. As its name indicates, a critical factor for MALDI to work as an ion source is an appropriate matrix. This refers to presence of a small organic acid or base in prepared samples that strongly absorbs light at the wavelength of the applied laser, thereby enabling both desorption and ionization of targeted analytes. The analyte-matrix mixture is dried before analysis, leading to crystal formation. During sample analysis, pulses of laser radiation on the crystals cause excitation of the matrix molecules and their subsequent desorption from the sample surface and ionization (Figure 1). The laser wavelength varies from ultraviolet (UV) to infrared, although nitrogen (337 nm) and neodymium-doped yttrium aluminum garnet (Nd:YAG, 355 nm) UV lasers are most commonly used [20]. Owing to its minimal sample preparation requirements and high tolerance of potentially interfering species, e.g., salts and buffering compounds, the technique soon became a pow-

erful analytical tool. This led to a pioneering application as a molecular imaging method, demonstrating the potential of MALDI-MSI for mapping distributions of small proteins and peptides in several tissue types [6]. Soon its use was extended to wide arrays of analytes, including small molecules such as endogenous metabolites and drugs, quite often simultaneously [15,21-24]. Nowadays, MALDI-MSI can provide lateral resolution of 1-5  $\mu\text{m}$  [25,26] .

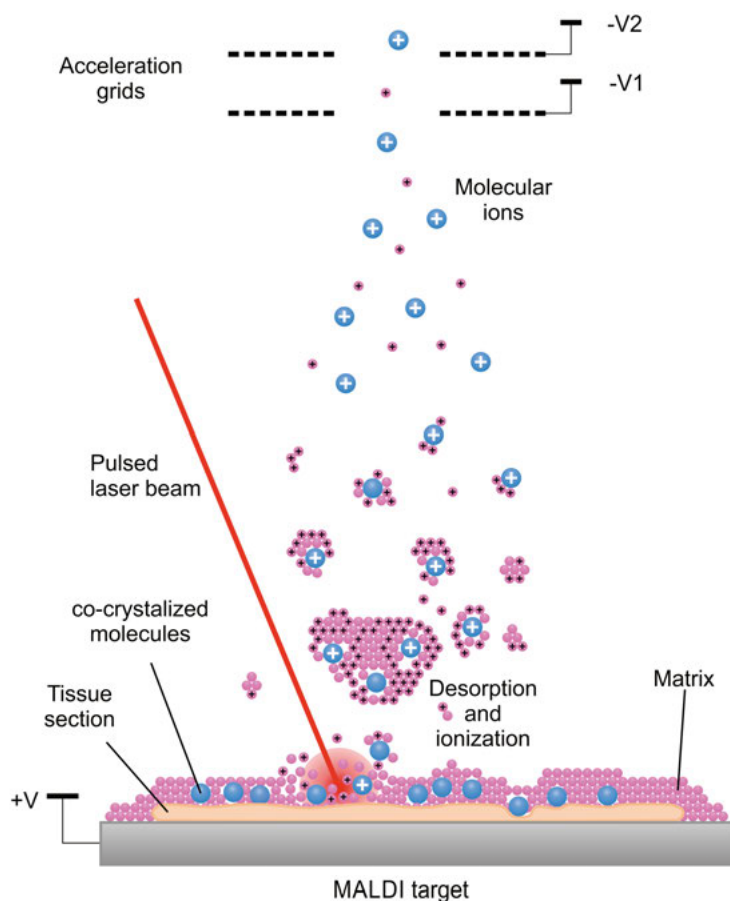


*Figure 1.* Schematic diagram of a MALDI ion source operating in positive ion mode. Laser radiation induces desorption/ionization of the matrix and co-crystallized analytes (the illustration is kindly provided by Dr. Patrik Källback).

### Desorption electrospray ionization

DESI is another ionization technique that is applied in MSI tissue distribution studies, which was introduced in 2004 [27]. In DESI, desorption and ionization of analyte molecules are facilitated by a high-velocity charged solvent stream directed onto the sample surface and the generated ions are

collected in an inlet capillary. During this process, geometric parameters of the DESI source including distances between the solvent sprayer, sample surface, and inlet capillary, as well as the corresponding angles should be optimized. Ionization is performed under atmospheric conditions and no matrix application is required. Recent instrumental advances have improved the lateral resolution achievable by DESI-MSI [28,29]. Less than 50  $\mu\text{m}$  is now routinely possible, but this is still lower than the resolution afforded by MALDI-MSI.

## MSI Instrumentation: Mass Analyzers

Between the ion source and detector, the generated ions must be separated according to their mass-to-charge ratios ( $m/z$ ) by the analyzer. There are various types of analyzers, based on different ion separation principles and functions, including quadrupole, ion trap (together with Orbitrap), time-of-flight (TOF), Fourier transform ion cyclotron resonance (FTICR), and hybrid instruments. Each type has specific advantages and limitations. The analyzers used in the MSI experiments included in the studies underlying this thesis are described below.

TOF analyzers separate ions after their initial acceleration by an electric field, according to their velocities when they drift in a free-field region. Their  $m/z$  ratios are determined by measuring the time they take to move through the free-field region between the source and the detector, since all ions are accelerated with the same kinetic energy. Owing to their function, TOF analyzers are suitable for pulsed and soft ionization techniques such as MALDI. In addition, the high frequencies of mass determinations per unit time provided by TOF analyzers significantly accelerate sampling speed. On the other hand, TOF instruments have lower mass resolving power than other analyzers, and mass shifts may occur during spectra acquisition due to unevenness of samples' surfaces.

A recently developed hybrid quadrupole-Orbitrap (Q-Exactive) instrument combines a quadrupole mass filter with an Orbitrap analyzer and FTICR technology [30]. It can provide high mass resolution (up to 280,000 at  $m/z$  200). However, it has lower sampling speed than TOF analyzers. Although it was initially developed for targeted and untargeted liquid chromatography/mass spectrometry (LC/MS) based proteomics, it has been successfully coupled to DESI-MSI.

In an ion cyclotron, ions are trapped in a circular trajectory in a magnetic field. Ions of a specific mass have a characteristic cyclotron frequency. In FTICR [31] analyzers the detector measures the cyclotron frequency of all the ions in the trap and uses a Fourier transform to convert these frequencies into  $m/z$  values. FTICR instruments have high mass resolving power, up to 10,000,000. However, they have longer analysis times than TOF instruments in MSI experiments.

## Brain Sample Preparation

In MALDI-MSI, the matrix molecules are applied on tissue sections, usually sectioned at a thickness of 8-14  $\mu\text{m}$  and mounted on an indium-tin oxide (ITO) coated glass slide. There are several matrix application approaches [32], but a matrix solution is often sprayed on dried tissue samples. A number of molecules have been used as MALDI matrices, the most widely applied including benzoic and cinnamic acid derivatives, such as 2,5-dihydroxybenzoic acid (DHB),  $\alpha$ -cyano-4-hydroxycinnamic acid (CHCA), and sinapinic acid, as well as 9-aminoacridine (9AA), a highly fluorescent dye. The optimal MALDI matrix strongly depends on properties of the analytes, for instance whether or not they have charged groups, their molecular weight, and the ionization mode (positive or negative).

However, some molecules are insufficiently ionized by the regular MALDI matrices, especially endogenous neurotransmitters, e.g., monoamines, aminoacids and their metabolites. Fortunately, derivatization targeting specific functional groups of these compounds, such as primary amines and/or phenols, has led to dramatic improvements in their limits of detection and, hence, enhancement of their comprehensive mapping in the brain [11,13,33]. Moreover, the developed derivatizing agents do not require further matrix application. The reaction mechanisms involving some of these derivatization agents, mainly pyrylium salts, such as 2,4-diphenylpyranium tetrafluoroborate (DPP-TFB) and fluoromethyl pyridinium derivatives, e.g., FMP-10, are illustrated in Figure 2.

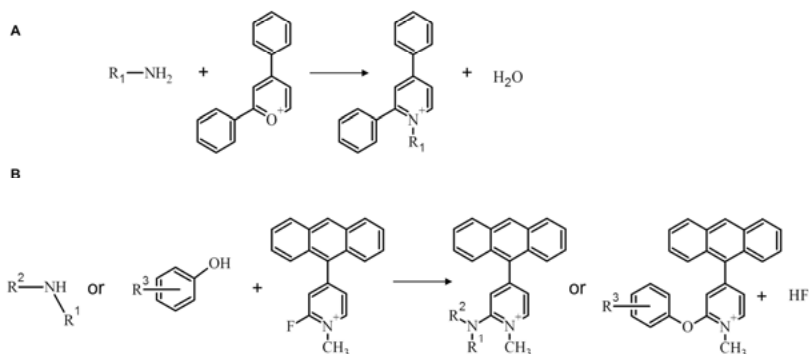


*Figure 2.* Schematic reaction between A) DPP-TFB and primary amines and B) the FMP-10 reactive matrix and hydroxyl phenols and amines. R1, R2 and R3 denote variable substituents.

Minimal sample preparation is required for a DESI-MSI analysis, compared to a corresponding MALDI-MSI analysis, since no matrix application is required. Nonetheless, the simultaneous mapping of neurotransmitters and

neuroactive substances in brain tissue has been achieved with a previously described derivatization approach [14].

Due to the differences in ionization efficiencies towards a wide range of analytes, these two ionization techniques can be complementary. The common experimental workflow for both techniques is briefly depicted in Figure 3.

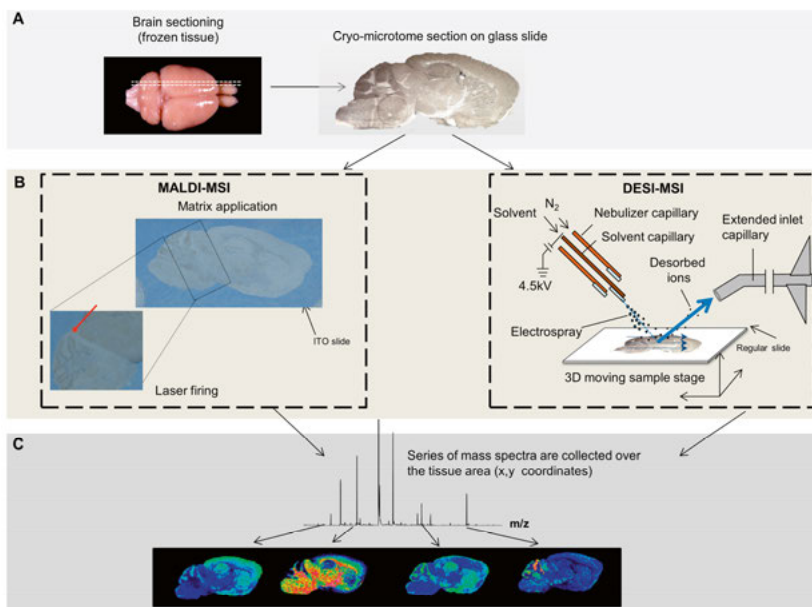


*Figure 3.* Summary of the experimental workflow of MALDI and DESI-MSI. A) Sectioning of frozen tissue samples. B) MALDI (left) and DESI (right) MSI analysis. C) Acquisition and visualization of MSI data. For every pixel analyzed, a mass spectrum is collected. An ion distribution image of the tissue section can then be obtained for each  $m/z$  signal present in the average spectrum.

## MSI Data Analysis

As thousands of ions can be simultaneously detected in MSI experiments, and their distributions can be visualized in pre-defined pixels in images of sections of tissues, inevitably big data files are generated. In addition, the complexity of the analyzed samples, presence of interfering molecules and instrumental artifacts, such as possible mass shifts, can generate biologically irrelevant variation, “noise”. Therefore, robust and time efficient tools for processing the acquired data and their biological interpretation are required.

Data processing steps usually include baseline correction/subtraction, spectrum smoothing and recalibration, and data normalization [34]. Normalization has emerged as a very important element of reliable MSI analysis. The total ion count (TIC) and root mean square of all data points (RMS) are

the most widely applied methods for normalization, especially of MALDI-MSI data. The use of internal standards has been proposed as a reliable normalization approach, but it is not always applicable, particularly for multiple analytes. Visualization of the MSI data is a very important process, and several software packages have been developed for this purpose, both commercial, e.g., flexImaging and SCiLS Lab, and open access, e.g., msiQuant [35,36], MSiReader, and Cardinal [37]. Staining of the tissue sections (hematoxylin and eosin, H&E, or Nissl), either the same sections following the MSI analysis or using consecutive sections, can significantly aid the delineation of specific tissue structures, especially in brain imaging. Successful definition of the brain areas of interest is a crucial step not only for the visual evaluation and interpretation of the data, but also for further statistical analysis or quantification.

There have been significant advances in MSI techniques for quantifying drugs and endogenous compounds in tissue sections in recent years. One of the first applications of quantitative MALDI-MSI was on lung tissue [38]. Since then, intense efforts have been made to optimize the experimental conditions, minimize error sources, estimate reliable pixel numbers, and identify appropriate normalization methods to develop and validate robust MSI methods [35,36,39,40]. The complexity of brains, which include various anatomically, functionally and molecularly distinct regions, should also be considered, especially regarding application of calibration curves. Free software now available can aid MSI quantification, and is applied on a routine basis [35,36].

Despite the wide use of univariate statistical methods in most biological investigations, multivariate analysis can be extremely valuable, especially for MSI datasets due to their scale and complexity [34,37,41-45]. Multivariate methods, particularly projection-based approaches such as Principal component analysis (PCA) and partial least squares-projection to latent structures (PLS), can tolerate big datasets with fewer objects than variables, as well as missing data [46,47]. They have been widely applied for identifying biomarkers of several (patho)physiological states in metabolomic, proteomic and genomic studies [48-50]. Owing to the extraction of orthogonal components, PCA, an unsupervised statistical method, has high potential ability for discriminating noise from biologically relevant variance, thereby revealing the main patterns in the data. However, the supervised extension methods of PCA, i.e., PLS and PLS-discriminant analysis (PLS-DA), can lead to overfitted models that fail to predict new data. Therefore, rigorous model validation approaches should be applied [51,52] and the data should also be appropriately visualized in MSI analyses.

## Neuroactive molecules in the brain

### Brain pharmacokinetics: drug transport through the brain barriers and distribution in the CNS

To exert any pharmacological effects in the brain, drugs must first enter the brain parenchyma by passing through the BBB [53]. The BBB is formed by the tight junctions of endothelial cells that line the wall of brain capillaries. These junctions limit fenestration, making transcellular diffusion the main transport pathway, while intercellular and paracellular ways (transcytosis and pinocytosis) are much less important [53,54]. Maintenance of the BBB is considered to be aided by the astrocyte end-feet and pericytes encircling the endothelial cells [54,55]. Notably, however, BBB integrity is not entirely uniform, with brain capillaries exhibiting a higher degree of permeability in specific areas adjacent to the ventricles, the so-called circumventricular organs (e.g., area postrema, neurohypophysis), as well as in newly formed blood vessels within brain tumors [56].

Another important feature of the BBB is the expression of membrane transporters, which contribute to brain transport of several endogenous and exogenous compounds [53,54]. Efflux membrane transporters, such as ATP-binding cassette (ABC) transporters, can further limit entry of molecules into the brain tissue. P-glycoprotein, also known as multidrug resistance 1 protein (MDR1) or ATP-binding cassette sub-family B member 1 (ABCB1), is one of the most important and commonly investigated ABC transporters [53,54,56,57]. Breast cancer resistance protein (BCRP/ABCG2) has also been extensively studied [58,59]. On the other hand, endogenous compounds and nutrients necessary for brain functions are transported into the brain by members of the solute carriers family, such as glucose transporter 1 (GLUT1), large neutral amino acid transporter (LAT1) and organic cation/carnitine transporter 2 (OCTN2) [53,60]. These transporters have also been shown to facilitate transport of several drugs into the brain [60,61]. A number of drug-metabolizing enzymes, such as P450 phase I and phase II enzymes have also been identified in the BBB [62]. Clearly, therefore the role of BBB is to protect the CNS from potentially toxic agents, as well as to maintain its homeostasis [54].

The blood-cerebrospinal fluid barrier (BCSFB), which constitutes a second interface, is formed by epithelial cells of the choroid plexus facing the cerebrospinal fluid (CSF) and joined together by tight junctions [53,54]. Notably, unlike the BBB, the choroidal epithelium serves as a barrier while the choroidal endothelium is fenestrated, allowing small molecules to diffuse into the interstitial space [63-66]. The choroid plexus is located in the brain ventricles and secretes the CSF. Some ABC transporters reportedly show differential expression or membrane localization in the choroid plexus and BBB, leading to higher concentrations of their substrates in the CSF than in

brain tissue [56,67]. A graphic illustration of the two barriers is given in Figure 4.

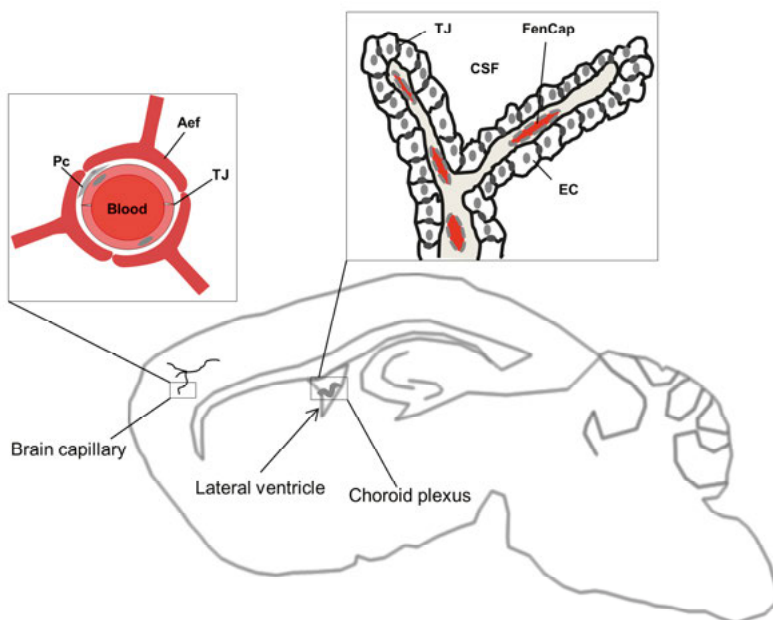


*Figure 4.* Graphic illustration of the brain barriers on a sagittal mouse brain tissue section. Abbreviations: Aef, astrocyte end foot; CSF, cerebrospinal fluid; EC, epithelial cell; FenCap, fenestrated capillary; Pc, pericyte; TJ, tight junction

Once a drug has entered the brain, its intra-brain distribution is governed by nonspecific binding, accumulation in particular intracellular compartments (e.g., basic lipophilic drugs in acidic lysosomes), carrier-mediated cellular influx/efflux, and interaction with its molecular target [68]. According to the free drug hypothesis, the concentration of unbound drug is the pharmacologically relevant concentration as it drives all distribution processes [69].

To date, the gold standard for quantifying BBB permeability and brain exposure has been *in vivo* cerebral microdialysis. Although the technique is accurate, reproducible, and suitable for measuring unbound drug concentrations in the brain [69], it is technically demanding and laborious [70]. A more high-throughput technique for studying drug distributions in the CNS is the brain slice method, which indicates the unbound brain volume of distribution [71]. However, neither approach can provide detailed localization information. Imaging techniques, such as positron emission tomography (PET), can provide valuable complementary quantification and localization information at sub-nM levels [72]. The use of radiolabeled isotopes involved hinders the differentiation of parent compounds from their metabolites and the spatial resolution provided by PET remains limited [72,73].

High-throughput methods based on *in vitro* and *in silico* tools, have also been developed for estimating BBB permeability. The most common *in vitro*

method is to measure the transendothelial electrical resistance, which indicates the tightness of endothelial junctions [74]. Although screening cell lines derived from several species are available [74], human immortalized endothelial cell line (hCMEC/D3) has been widely used as an *in vitro* human BBB model [75]. Monolayers of these cells express the characteristic BBB tight junction proteins, e.g., adheren proteins, claudin-3 and occludins, with transendothelial electrical resistance measurements being highly dependent on the co-culture of astrocytes and pericytes [75,76]. hCMEC/D3 expression of transporter proteins has further improved the performance of these models [77]. However, due to high dependence of the measured data on the experimental conditions and model properties, further developments are required [74]. *In silico* approaches have indicated molecular and physicochemical properties related to high or low BBB permeability, as well as structural features enabling interactions with the major BBB transport proteins [78-81]. Despite the time and cost efficiency provided by these methodologies, they do not provide important biological information and are mainly applicable in initial screening of drug libraries.

Membrane transporter-induced drug-drug interactions (DDIs) have also been examined in a high-throughput manner *in vitro* [80]. In addition, modified cell lines with high expression of efflux transporter proteins have been successfully used in conjunction with transporter inhibitors for rapid examination of membrane permeability [82,83].

## Brain pharmacodynamics: molecular neuropharmacology and major neurotransmitter systems

Most common drug targets in the CNS include receptors (in cell membranes or intracellular), enzymes (such as esterases, protein kinases, oxidases, and phosphatases), and neurotransmitter transporters. Neuroactive drug-target interactions usually lead to some modification of the neurotransmission process, either through a presynaptic effect, involving changes in the synthesis, storage, release, or termination of the neurotransmitter's action, or postsynaptic. The major neurotransmitters affected by pathological neural states and involved in the pharmacology of most clinically used drugs include the catecholamines, e.g., dopamine (DA) and norepinephrine (NE), serotonin (5-HT),  $\gamma$ -aminobutyric acid (GABA), and acetylcholine (ACh).

ACh, the neurotransmitter of the cholinergic system, was the first chemical neurotransmitter to be identified, in 1921 by the pharmacologist Otto Loewi [84]. The synthesis, storage, release and metabolism of ACh have been extensively investigated. ACh is synthesized in the presynaptic terminals via a reversible reaction, catalyzed by choline acetyl transferase (ChAT), in which an acetyl group is transferred from acetyl-coenzyme A to choline [85]. There are two types of neurons in the cholinergic system: so-

called interneurons — local circuit cells occurring in the caudate putamen (CPu), nucleus accumbens (Acb), olfactory tubercle (Tu), and islands of Calleja [86,87]— and the projecting cholinergic neurons. The latter are divided into the basal forebrain cholinergic complex — medial septal nucleus, diagonal band nuclei, substantia innominata, magnocellular preoptic field, nucleus basalis — and the brainstem cholinergic nuclei (pedunculopontine nucleus and laterodorsal tegmental nucleus) [88,89]. They both have projections that extend to all major limbic structures, such as the hippocampus (Hip) and amygdala (Amy), and to the neocortex [90].

ACh effects are mediated by two types of receptors, the muscarinic and nicotinic cholinergic receptors [88]. Depending on the type, activation of cholinergic receptors has been shown to have a positive or negative effect on DA release [91]. Cholinergic transmission through the hippocampal formation and medial prefrontal cortex is particularly vital for cognitive function [92]. The actions of ACh are terminated by acetylcholinesterase (AChE), a highly active enzyme that hydrolyzes ACh into acetate and choline and can be found in the cytoplasm and outer cell membrane. Loss of cholinergic neurons in the mentioned brain regions is associated with pathological neurodegenerative states such as dementias, including Alzheimer's disease (AD) [93]. The most widely applied therapeutic regime for AD is administration of AChE inhibitors to decrease rates of ACh metabolism to choline and thereby increase levels of available ACh in the synapses.

Historically, the monoaminergic neurotransmitters (DA, NE, 5-HT) have been of high interest in neuropharmacology and a growing body of recent evidence indicates there are significant interactions among them. The main DA pathways in the CNS are the nigrostriatal and mesocorticolimbic pathways, with DA projections from the substantia nigra pars compacta (SNc) to the dorsal striatum (CPu), and from the ventral tegmentum (VT) to prefrontal cortex and ventral striatum (Acb and Tu), respectively [94]. The nigrostriatal pathway is responsible for voluntary motor control and is significantly affected in Parkinson's disease (PD), in which progressive loss of DA neurons in the SNc occurs [95]. Hence, current PD treatment approaches include DA replacement therapies, such as administration of L-DOPA (the DA precursor) or DA receptor agonists. The mesocorticolimbic pathway is considered to be related to cognition and reward mechanisms, and involved in disorders such as schizophrenia and addiction [96]. However, recent studies have reported significant intermixing of DA neurons projecting to different target structures [97]. In addition, there are increasing indications of significant DA transmission and neuronal activity in functions of other brain structures, such as the Hip and specific thalamic nuclei. Interestingly, DA release from noradrenergic neurons of the locus coeruleus (LC), the major NE projecting structure, in the dorsal Hip, enhancing spatial learning and memory, has been recently reported [98].

NE and 5-HT neurons project more broadly and in less defined pathways [99]. NE neurons project from the LC to the cortex (Cx), Amy, Hip, thalamus (Th), hypothalamus (Hyp), and cerebellum (Cb), but not the striatum (Str). Important roles of NE in cognition, arousal, attention and behavior have been established [100]. The 5-HT containing nuclei can be divided into two groups: the rostral group in the midbrain and rostral pons (caudal linear, dorsal and medial raphe nuclei), and the caudal group in the caudal pons and medulla (raphe magnus, obscurus and pallidus and lateral medullary reticular formation) [101]. Both groups project to the brainstem, i.e., midline thalamic nuclei and Hyp, while the former exhibits major projections in the forebrain, including cortical areas, Hip, entorhinal cortex and amygdalar nuclei. The VT and LC (containing DA and NE releasing neurons, respectively) receive serotonergic innervation too [102,103]. 5-HT is also a modulator of cognition, memory, learning and reward.

Unlike ACh, the reuptake via membrane reuptake transporters of monoaminergic neurotransmitters released by a neuron, is the major mechanism of their inactivation in the brain [104]. Inhibition of these transporters is a well-established approach in the treatment of mood disorders, such as depression, while many of the neuroleptic drugs act by blocking the monoamine receptors [104].

GABA is the main inhibitory neurotransmitter of the CNS, and it is much more abundant in the brain than the monoamines (total contents: millimoles and nanomoles, respectively)[105]. GABA has a primary role in inhibitory control of the dopaminergic system [106]. Inhibitory GABAergic outputs originating in the CPu terminate in the internal part of the globus pallidus and substantia nigra pars reticulata.

This brief overview clearly shows that there are essential interactions among the neurotransmitters, and they exert highly region-specific effects. Both of these features add to the complexity of the CNS. Current methods for identifying and mapping their pathways and distributions are usually based on indirect analyses, involving detection of enzymatic markers, such as ChAT or AChE for the cholinergic system.

## Neuroimaging of age-induced alterations

The discovery of neuropathological anatomic landmarks, for instance the accumulation of beta-amyloid plaques in AD and Lewy bodies in PD, has enabled great advances in the diagnosis of neurodegenerative diseases. However, the etiopathogenesis of most neurological conditions remains unknown.

Since aging is widely considered the major risk factor for neurodegenerative diseases such as AD and PD [107,108], the delineation of cellular senescence mechanisms can offer important insights into degeneration. Most approaches are based on untargeted metabolomic analyses using LC/MS to

identify and quantify small molecules affected by aging in large pools of endogenous metabolites [109]. However, this technology cannot provide detailed brain localization information, which is essential for understanding neuronal senescence. In addition, it is important to incorporate neuroimaging approaches in drug discovery and development [110].

Magnetic resonance spectroscopy, a non-invasive imaging technique, has been applied in studies of both normal human brain aging and neuropathological conditions [111,112]. However, it provides limited spatial resolution (usually around  $0.25\text{ cm}^3$ ) [112,113], and the range of the investigated brain metabolites is relatively narrow, including highly abundant CNS molecules such as N-acetylaspartate, choline, and creatine [111,112]. Nonetheless, the ability to detect a broad spectrum of molecules simultaneously is important since brain aging is a multifactorial process affecting levels of a wide range of biomolecules that play crucial roles in neuronal signaling, including neurotransmitters [114,115], transporters [116,117], receptors [118,119], and metabolizing enzymes [120].

Age-induced alterations have been detected in multiple neurotransmitter systems. The cholinergic system has been extensively studied in relation to aging [93,121]. Dopaminergic alterations triggered by aging have been linked to motor symptoms [122], the reward system [123], working memory, and cognitive functions [124,125]. In addition, age-related decline in the activity of noradrenergic neurons in the rat LC has been associated with cognitive age-related decline [124,126], deterioration of serotonergic neurotransmission with development of age-related depression [127], and decreases in histamine (His) receptors with impairment of attention and cognition [128]. Moreover, age-induced changes in critical metabolic processes, including mitochondrial function and lipid signaling, have been reported, although much remains to unveil.

As described in the previous paragraph, each neurotransmitter is involved in different pathways, located in numerous brain areas and interconnected with each other. Detailed analysis of neurochemicals' distributions in healthy physiological states and changes in their distributions in pathological states is, therefore, crucial.

# Aims

In the studies this thesis is based upon (reported in four appended papers, designated Papers I-IV), we exploited the advantages and improvements of MSI in neuropharmacology aiming to:

- establish an MSI approach for assessing the BBB permeability and brain localization of several well-characterized pharmaceutical compounds and investigate potential DDIs at the BBB (Paper I);
- investigate how normal aging affects the levels and responsiveness of the cholinergic system to AChE inhibition by tacrine, and the brain distribution and metabolism of the drug (Paper II);
- detect age-induced modifications and perturbations in multiple metabolic pathways in the brain, including mitochondrial function, neurotransmission, and lipid signaling, as well as responses of these systems to AChE inhibition (Paper III);
- further investigate region-specific responses of multiple neurotransmitter systems, such as the dopaminergic, noradrenergic, serotonergic, GABAergic, and histaminergic systems, to aging and AChE inhibition (Paper IV).

# Methods

## Animal experiments

All experiments complied with European Council Directive (86/609/EEC) and were approved by the local Animal Ethics Committee (approval nos. N40/13 and N275-15). Efforts were made to minimize the number of animals used and their suffering. All mice were housed under controlled temperature and humidity, with 12 h light/12 h dark cycles and *ad libitum* feeding.

Adult male C57Bl/6J or Swiss mice, approximately 4 months old (average body weights  $24.8 \pm 1.4$  g and  $43.9 \pm 2.3$  g, respectively), supplied by Janvier labs, Scand-LAS Turku, Finland, were used in Study I. Propranolol ( $n=3$ ) and loperamide ( $n=3$ ) were administered intraperitoneally (i.p.) at doses of 10 and 5 mg/kg, respectively. In a co-administration experiment, six animals were pre-treated with a 5 mg/kg intravenous injection (i.v.) of elacridar 30 min before administration of either propranolol ( $n=3$ ) or loperamide ( $n=3$ ), both of which were administered via the same route and at the same dose as when administered alone. Control animals were injected with an equivalent amount of vehicle solvent (saline and 5% Tween 80 in experiments with propranolol and loperamide, respectively). In both dosing regimens, i.e., with and without elacridar, animals were sacrificed by decapitation 30 min and 1 h after the administration of propranolol and loperamide, respectively.

Male C57BL/6J mice, aged 12 weeks (12-w,  $n=8$ ) and 14 months (14-m,  $n=8$ ), also supplied by Janvier labs, Scand-LAS Turku, Finland, were used in Studies II-IV. Tacrine, dissolved in saline, was administered i.p. at a dose of 10 mg/kg to both 12-w and 14-m mice. Control 12-w and 14-m animals were injected with an equivalent amount of vehicle. All animals were euthanized by decapitation 30 min after the injection.

In both experiments, brains were then rapidly dissected out, snap-frozen in dry-ice cooled isopentane, and stored at  $-80$  °C.

## Tissue processing

### Tissue sectioning

All brain tissue samples sectioned at  $-20\text{ }^{\circ}\text{C}$  using a cryostat-microtome (CM3050S in Study I and CM1900 UV in Studies II-IV, both supplied by Leica Microsystems, Wetzlar, Germany) after equilibration at this temperature. Brain tissue sections, coronal and sagittal, were cut at a thickness of  $14\text{ }\mu\text{m}$  (Study I) or  $12\text{ }\mu\text{m}$  (Studies II-IV) and subsequently thaw-mounted either on SuperFrost glass slides (Menzel-Glaser, Braunschweig, Germany) for DESI-MSI analysis (Study I) or conductive ITO-coated glass slides (Bruker Daltonics, Bremen, Germany) for MALDI-MSI experiments. Multiple coronal and sagittal brain levels were collected for comprehensive analysis of the tissue distribution of analytes in several brain structures [129]. The slides were stored at  $-80\text{ }^{\circ}\text{C}$  and the sections were desiccated at room temperature for 15 min prior to analysis. Slides were imaged optically using a photo scanner (Epson Perfection V500, Japan).

### Quantification of drugs and neurotransmitters

#### **Calibration curve application**

For the quantification of propranolol and loperamide in brain tissue, six standard solutions of each compound were prepared in 50% methanol and spotted (at 100 nL per spot), together with a blank, on control mouse brain sections using an automated spotter (Preddator, Redd&Whyte Limited, Suffolk, UK). The concentration ranges for propranolol and loperamide were  $19.8\text{ }\mu\text{M}$ - $0.6\text{ }\mu\text{M}$  and  $1.35\text{ }\mu\text{M}$ - $0.04\text{ }\mu\text{M}$ , respectively, with a dilution factor of two (Study I).

For the quantification of ACh levels in brain tissue, six standard solutions of deuterated ACh (ACh- $d_4$ ) (2.00, 1.50, 1, 0.50, 0.25, and  $0.125\text{ }\mu\text{M}$ ) were prepared in 50% methanol with 0.2% trifluoroacetic acid (TFA) and spotted (at 50 nL per spot), together with a blank (50% methanol, 0.2% TFA) on control (12-w and 14-m) coronal mouse brain sections using a CHIP-1000 chemical inkjet printer (Shimadzu Corporation, Tokyo, Japan) (Study II).

Tacrine concentrations in brain tissue were estimated using a series of five standard solutions (5.00, 2.50, 1.25, 0.63 and  $0.31\text{ }\mu\text{M}$ ) manually spotted (at  $0.1\text{ }\mu\text{L}$  per spot) on control brain tissue (Study II).

Spots for the standard calibration were preferably applied to the cortical area, to keep tissue matrix suppression effects as constant as possible.

#### **Internal standard application**

Internal standard solutions of deuterated analogues of the analytes, applied with an automatic sprayer (TM-sprayer, HTX-Technologies LLC, Chapel Hill, NC), were used for data normalization. Concentrations were adjusted

depending on estimated analyte concentrations in the tissue. Propranolol- $d_7$  (3.00  $\mu\text{M}$ ) and loperamide- $d_6$  (0.08  $\mu\text{M}$ ), dissolved in 50% acetonitrile with 0.2% TFA, were the internal standards used for analyzing samples from mice that had been administered propranolol and loperamide, respectively (Study I). Solutions of the deuterated standards were sprayed in six passes at 80 °C., ACh- $d_9$  (0.367  $\mu\text{M}$ ) solutions in 50% acetonitrile and 0.2% TFA, applied in six passes at 90 °C, were used as the internal standard for the MALDI-MSI analysis of ACh (Studies II and III).

Owing to its structural similarity, 9-aminoacridine (9AA) was used as the internal standard for the MALDI-MSI analysis of tacrine and its hydroxylated metabolites and 9AA solutions (1.464  $\mu\text{M}$ ) in 50% acetonitrile with 0.2% TFA were sprayed in six passes at 90 °C (Study II).

In every application of internal standard, a solvent flow of 70  $\mu\text{L}/\text{min}$ , nozzle velocity of 1100 mm/min, and track spacing of 2.0 mm were used.

## Preparation of brain tissue sections

### Matrix application

Before MALDI-MSI data acquisition, a matrix solution was applied (using the previously described automatic sprayer) to the dried brain tissue sections after the internal standard application, when performed.

The MALDI matrix selection was based on examination of the ionization/desorption efficiency (signal-to-noise ratio and presence of interfering peaks) of the analytes using different matrices in both positive and negative ion modes. DHB dissolved in 70% acetonitrile with 0.2% TFA at 35 mg/mL, was used as the matrix for MALDI-MSI of sphingomyelin species in the choroid plexus (Study I). A slightly different DHB solution (35 mg/mL in 50% acetonitrile/water with 0.2% TFA) was used for the MALDI-MSI of tacrine and its hydroxylated metabolites (Study II), and in the untargeted analysis (Study III). The DHB matrix solutions were applied with the TM-sprayer at 95 °C, in six passes at a solvent flow of 70  $\mu\text{L}/\text{min}$ . The nozzle velocity was 1100 mm/min and track spacing 2.0 or 3.0 mm.

Deuterated CHCA (CHCA- $d_4$ ) [12] was used as the matrix for the MSI analysis of ACh brain levels and distributions (Studies II and III) and untargeted analysis (Study III). A 5 mg/mL solution of CHCA- $d_4$ , dissolved in 50% acetonitrile with 0.2% TFA, was applied using the same method as for the internal standard application.

### On-tissue derivatization

On-tissue chemical derivatization with DPP-TFB (Study III) and FMP-10 (Studies III and IV) was performed according to protocols developed in our lab [11,33]. Briefly, DPP-TFB (1.3 mg/ml) was dissolved in 75% methanol and alkalified with 3.5  $\mu\text{l}$  of triethylamine. FMP-10 was dissolved in 70%

acetonitrile to a concentration of 4.4 mM. Both matrices were sprayed on mouse brain tissue sections using the TM-sprayer at 80 °C in 30 passes with a flow rate of 80  $\mu$ L/min, nozzle velocity of 1100 mm/min and track spacing of 2.0 mm. In DPP-TFB derivatization, after matrix application the samples were incubated for 15 min (dried under a nitrogen stream every 5 min) in a chamber saturated with the vapor arising from a 50% methanol solution.

## Mass Spectrometry Imaging

A modified DESI source (Prosolia OmniSpray 2D, Indianapolis, IN, USA) mounted on an Orbitrap mass spectrometer (Q-Exactive, Thermo Scientific, Bremen, Germany) was used to acquire DESI-MSI data [27,130] (Study I). Geometric parameters of the DESI source and other relevant instrument parameters were optimized and adjusted to collect a maximum number of ions while avoiding detector saturation. Positive ionization mode was used for the DESI-MSI with propranolol and loperamide, while negative ionization mode was used for elacridar analysis. MS/MS spectra of loperamide and elacridar were acquired using a 2.0 Da isolation window ( $\pm$ 1.0 Da around target mass).

MALDI-MSI of the sphingomyelin species was performed using a MALDI-TOF/TOF (ultrafleXtreme and rapifleX, Bruker Daltonics) mass spectrometer in positive ionization mode (Study I). The laser power was optimized at the start of each run. On-tissue MS/MS fragmentation experiments were performed using MALDI-TOF/TOF in positive ionization mode with a 6.0 Da isolation window ( $\pm$ 3.0 Da around target mass).

In Studies II-IV, all MALDI-MSI experiments were performed using a MALDI- FTICR mass spectrometer (Solarix XR 7T- 2 $\omega$ , Bruker Daltonics) in positive ionization mode with a Smartbeam II 2 kHz Nd:YAG laser. Overall, the instrument was tuned for small molecules ( $m/z$  86-1000), while the transfer optics parameters were set according to the  $m/z$  range of target analytes. Continuous accumulation of selected ion (CASI) was used in some analyses of selected analytes, such as ACh and tacrine, to improve the limit of detection. On-tissue MALDI-MS/MS fragmentation experiments were performed by isolating the precursor ion in a window of 1-18 Da, depending on the analyte, allowing the target ions to be selected in the quadrupole and accumulated in the collision cell. In certain cases, wider mass windows allowed better sensitivity. The collision energy voltages ranged from 10 to 35.0 V, depending on the precursor ion.

## Histological staining of tissue sections

Mouse brain tissue sections on the same slide were histologically stained after MSI analysis to assist delineation of brain structures. For this, digital images of H&E stained sections were captured using a slide scanner (Nano-Zoomer 2.0, Hamamatsu, Japan) and Aperio ImageScope v12.2.2.5015 software (Leica) following DESI-MSI (Study I). In Studies II-IV, digital images of Nissl stained sections were captured using a photo scanner (Epson Perfection V500) after MALDI-MSI analysis.

## Imaging data analysis

DESI-MSI data processing and visualization (Study I) as well as quantification analysis (Studies I and II) were performed using msIQuant software (developed in-house) after converting the imzML data into the appropriate format [35,36].

MALDI-MSI data were visualized using flexImaging (v.5.0, Bruker Daltonics) and further analyzed by SCiLS Lab (v. 2019a Pro, Bruker Daltonics) (Studies II-IV).

The MSI data were normalized using a deuterated internal standard, when available. Normalization with respect to the RMS of all data points and TIC was applied to full mass range FTICR and TOF/TOF MALDI-MSI data, respectively. However, no normalization was applied to DESI-MSI data and CASI-acquired MALDI-MSI data with no internal standard.

Brain structures were annotated using a mouse brain atlas [129], assisted by the H&E or Nissl staining. Normalized average ion intensities were extracted from each defined region of interest in SCiLS Lab and subsequently log-transformed for further statistical analysis.

## Statistical analysis

In Studies I-IV, univariate and multivariate statistical methods were used depending on the question addressed and nature of the data. Normality (Shapiro-Wilk) and homogeneity (Levene's) tests were initially applied. To examine the effect of elacridar administration on brain transport of propranolol and loperamide, a one-sample t-test, with the significance threshold set to  $P < 0.05$ , was applied (SPSS, v. 22.0, IBM, Armonk, NY, USA) (Study I). Two-way ANOVA with the significance level ( $\alpha$ ) set at 0.05 and Tukey's post hoc testing was applied to assess effects of tacrine administration and age, expressed as binary (2-level) factors, on ACh levels (Study II).

Multivariate data analysis (MVDA, with SIMCA v.13.0 software, Sartorius Stedim Biotech, Umeå, Sweden) was mainly used to detect significant

changes in levels of small metabolites and neurotransmitters in multiple brain structures associated with aging and/or tacrine administration (Studies III and IV). PCA was initially applied to obtain an overview of the data and identify possible outliers. Subsequently, four age- and treatment-associated classes of samples were defined: 12-w and 14-m control (saline-injected) mice, and 12-w and 14-m tacrine (tacrine-administered) animals. PLS-DA was then used to reveal specific differences among the groups. Well-established validation procedures were applied to evaluate the results [52,131] as well as two-way ANOVA with Tukey's post hoc analysis.

## Identification of metabolites

Biologically significant detected ions were primarily annotated by database searches, based on the mass accuracy obtained by FTICR MS analysis ([www.hmdb.ca](http://www.hmdb.ca), [www.lipidmaps.org](http://www.lipidmaps.org), [metaspace2020.eu](http://metaspace2020.eu)). Subsequently, standards were used to confirm the identifications, when available. MALDI-MS/MS was performed on-tissue and the derived product ions were compared to product ion spectra of standards or previously published data and, in samples subjected to MS/MSI analyses, their brain tissue distributions of the product ions were compared to distributions of the parent molecules. The presence of primary amine and/or phenolic groups, confirmed by their specific derivatization by DPP-TFB and/or FMP-10, also aided the identification of particular molecules.

## Permeability screening study and *in vitro* transport experiments

*In vitro* permeability and transport experiments were carried out to explain and confirm MSI data. Effects of elacridar on transport of propranolol and loperamide were further examined in Madin-Darby canine kidney II cells (MDCK) with canine MDR1 transporter knockout (MDCK<sup>cMDR1-KO</sup>) [82,83] and MDCK cells overexpressing human MDR1 transporter (hMDR1) with cMDR1 knockout (MDCK-hMDR1<sup>cMdr1-KO</sup>) (Study I). The interaction and active uptake of tacrine and its hydroxylated metabolite with the novel organic cation/carnitine transporters 1 and 2 (OCTN1, OCTN2) were assessed by inhibition and uptake experiments with human embryonic kidney 293 (HEK293) Flp-In cells stably overexpressing OCTN1 or OCTN2 transporters (kindly provided by Prof. Kathleen Giacomini, University of California, San Francisco). Total protein content was measured using a protein assay reagent kit (Pierce BCA Protein Assay Kit, Biotechnology, Rockford, IL) according to the manufacturer's instructions and the resulting protein con-

centrations were used for normalization of the cellular uptake. A LC-MS/MS instrument (Acquity UPLC-TQ MS, Waters Corp., Milford, MA) was used to measure intracellular levels of compounds used in the tests.

# Results and Discussion

In the studies underlying this thesis, the brain tissue distributions of *in vivo* administered compounds (propranolol, loperamide and elacridar in Study I and tacrine in Studies II and III), as well as endogenous small molecules present in the CNS (neurotransmitters and their metabolites, amino acids, lipids, metabolic intermediates, dipeptides in Studies III and IV) were investigated by MSI. Chemical structures of the administered compounds and the major investigated neurotransmitters are shown in Figure 5.

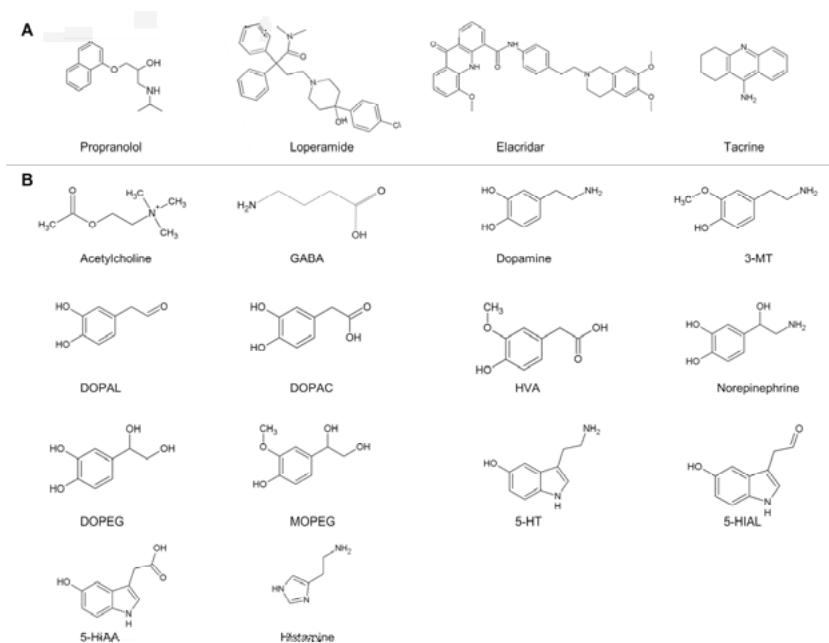


Figure 5. Chemical structures of representative analytes investigated in the present thesis.

## MSI of MDR1-mediated efflux effects on drug distribution in the brain (Paper I)

Brain transport of pharmaceutical molecules, a crucial factor to consider in the drug development process, was the focus of Paper I. In the reported

study, a DESI-MSI approach was developed to assess the BBB transport and brain localization of molecules with different BBB permeability profiles. In addition, the impact of MDR1-mediated DDIs on their distributions in brain tissues was investigated. Two marketed drugs, propranolol and loperamide, were used as model compounds and were administered to mice, either with or without co-administration of elacridar, a well-studied MDR1 inhibitor [132]. Membrane transport of propranolol has been shown to be primarily dominated by passive diffusion [57,133], whereas loperamide, a MDR1 substrate, has displayed restricted entry into the brain [57,134]. DESI-MSI was used to determine distributions and concentrations of propranolol and loperamide in several brain areas and estimate effects of MDR1 inhibition on their brain transport. The results were further supported by application of a recently developed permeability screening technique with a MDR1 (ABCB1) knockout MDCK cell line overexpressing human MDR1 [82,83,135].

### The highly permeable compound propranolol was distributed throughout the brain tissue

Propranolol readily entered into the brain, within 30 min after its i.p. administration. The concentration of propranolol ( $m/z$  260.1643) in brain tissue sections was highest in the grey matter (Cx, Hip, CPu, Th, and Hyp) and considerably lower in white matter areas (e.g., corpus callosum, cc and internal capsule, ic), as illustrated by DESI-MSI of a sagittal mouse brain tissue section at 100  $\mu\text{m}$  lateral resolution (Figure 6). This was also verified by quantification of brain levels of propranolol in the main representative fore-brain regions (Cx, CPu, and Hip), Th, Hyp, and white matter (cc, ic) (Figure 6C). Propranolol's high membrane permeability was corroborated by experiments with the recently developed modified MDCK cell lines overexpressing human MDR1 (hMDR1) transporter. The average efflux ratio (ER) obtained in these experiments was  $0.9 \pm 0.1$ , significantly lower than the  $\text{ER} \geq 2$  threshold, indicating no significant transporter involvement in its transport across the membrane.

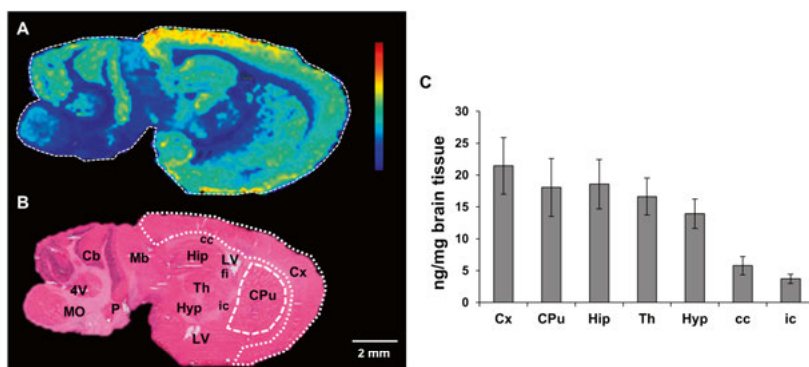


**Figure 6.** Brain distribution of propranolol after i.p. administration. A) DESI-MSI of propranolol ( $m/z$  260.1643, scaled to 30% of max intensity) on a sagittal mouse brain section at a lateral resolution of 100  $\mu\text{m}$ . B) The tissue section was subsequently washed and stained by H&E, and relevant brain structures of interest were annotated. The Cx and CPu are illustrated using white dashed lines. C) Absolute concentration of propranolol in specific brain regions. Error bars show the standard error of the mean ( $n=3$ ).

### Specific localization of loperamide in the choroid plexus as an indicator of limited entry into the brain parenchyma

Unlike propranolol, the only brain regions containing loperamide ( $m/z$  477.2304) following its administration were the ventricles, according to DESI-MSI of coronal mouse brain tissue sections at 100  $\mu\text{m}$  lateral resolution (Figure 7A). Higher lateral resolution DESI-MSI analysis (75  $\mu\text{m}$ ) revealed its specific localization in the choroid plexus, which constitutes the BCSFB (Figure 7B) and, to a much lower extent (approximately four-fold lower), surrounding ependymal cells and ventricular interior. This finding was further confirmed by the spatial co-localization of loperamide with the sphingomyelin species SM(d18:1/22:0), a lipid found to be specifically localized in the choroid plexus by a recent MSI study [136] (Figure 7C). In addition, the lack of spatial correlation between loperamide and heme, a marker of blood vessels [15,137], in the ventricular areas indicates that loperamide may have penetrated the fenestrated microvessels of the highly vascularized choroid plexus and passed into the epithelial cells.

The specific localization of a loperamide N-dealkylated metabolite, N-desmethyl loperamide, in the choroid plexus has also been reported in a previous PET study of human subjects following loperamide administration [138]. In addition, differences in expression patterns of the ABC transporters MDR1 and BCRP between the BCSFB and BBB may lead to higher concentrations of their substrates in the CSF than in brain tissue [56,67]. Finally, the average ER of loperamide in the transport experiments with the MDCK

cell line was around  $40 \pm 4.0$ , significantly higher than the  $ER \geq 2$  threshold, indicating involvement of an efflux transporter.

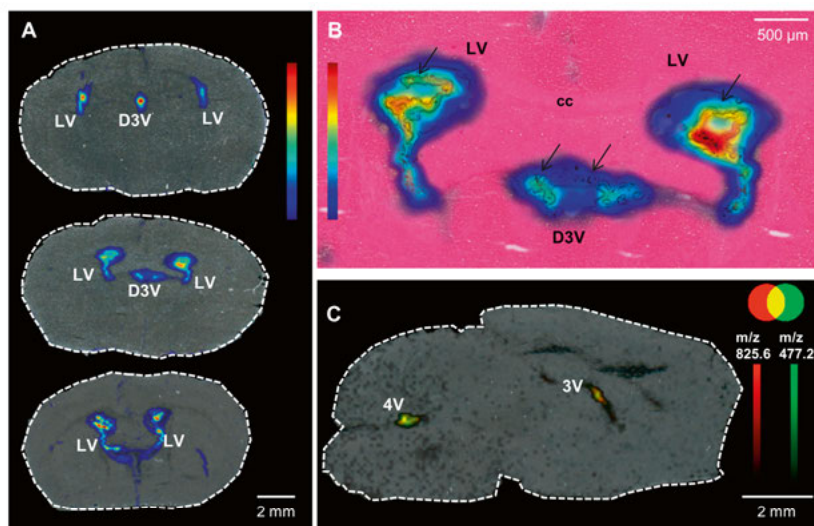


**Figure 7.** Localization of loperamide in the choroid plexus of the brain ventricles. A) DESI-MSI of loperamide ( $m/z$  477.2304, scaled to 30% of max intensity) shows distribution in the lateral and dorsal third ventricles of coronal brain sections, collected at three different brain levels (100  $\mu$ m lateral resolution). B) DESI-MS/MSI of loperamide ( $m/z$  266.1643, scaled to 30% of max intensity, 75  $\mu$ m lateral resolution) distribution overlaid with the subsequently H&E stained image using the image fusion function implemented in the msIQuant software [35]. The choroid plexus is annotated with arrows. C) Overlaid DESI-MSI distribution data of loperamide (green,  $m/z$  477.2) and the potassium adduct of SM(d18:1/22:0) (red,  $m/z$  825.6) on a sagittal brain section at 100  $\mu$ m lateral resolution. Abbreviations: 3V, third ventricle; 4V, fourth ventricle; D3V, dorsal third ventricle; LV, lateral ventricles; cc, corpus callosum.

## MDR1 inhibition-mediated DDIs at the BBB

The evaluation of DDIs during early stages of drug development is highly recommended [58]. The MDR1 transporter inhibitor elacridar was considered suitable for investigating MDR1 transporter-mediated DDIs, since it has shown weak interference with the major CYP isoforms involved in metabolism of loperamide and propranolol [139-141]. In Study I, elacridar was administered at a transporter inhibitory dose (5 mg/kg i.v.), which has been considered to increase the brain uptake of compounds that are MDR1 substrates [142].

Co-administration of elacridar did not significantly affect the brain distribution of propranolol, as illustrated by the coronal brain tissue sections (Figure 8A, B). On the contrary, and most importantly, MDR1 inhibition by elacridar notably increased levels of loperamide in various brain grey matter

structures (Cx, Hip, CPU, and Cb), about 3-fold, while maintaining relatively high abundance within the ventricles (Figure 8C, D).

The classification of loperamide as a MDR1 substrate and propranolol as a non-substrate was further corroborated by ERs obtained in experiments with the MDCK cell line in the presence of elacridar, as the ER of loperamide was close to zero with elacridar co-administration while the ER for propranolol was unaffected (Figure 8E).

Overall, this study illustrated the potential of MSI as an innovative imaging technique for characterizing distributions of drug molecules with varying BBB permeability in the brain. Most importantly, it demonstrated its applicability in DDI investigations.

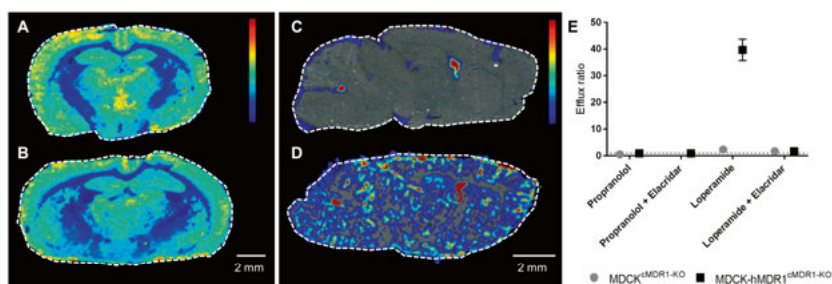


*Figure 8.* Impact of elacridar co-administration on the brain distribution of propranolol and loperamide. A, B) DESI-MSI of propranolol ( $m/z$  260.1643, scaled to 70% of max intensity) in coronal mouse brain sections without and with the co-administration of elacridar, respectively, at a lateral resolution of 100  $\mu\text{m}$ . C, D) DESI-MS/MS imaging of loperamide ( $m/z$  266.1537, scaled to 10% of max intensity) in sagittal mouse brain sections without and with the co-administration of elacridar, respectively, at a lateral resolution of 100  $\mu\text{m}$ . E) ERs for propranolol and loperamide in the MDCK<sup>MDR1-KO</sup> and MDCK-hMDR1<sup>MDR1-KO</sup> cells with or without addition of the MDR1 inhibitor elacridar. The dashed line indicates an ER of 1. Data are presented as mean standard deviation for one representative experiment performed in triplicates.

## Region-specific effects of aging and tacrine-induced AChE inhibition on multiple neurochemical systems (Papers II-IV)

As aging causes neurochemical alterations in the brain that are often related to changes in memory and cognitive performance, we investigated effects of normal aging on the neurotransmitters involved in several intellectual and emotional functions. Firstly, we focused on the cholinergic system, degeneration of which is observed in AD and related dementias [143]. These neurological dysfunctions are mainly treated with AChE inhibitors that increase availability of ACh in synapses [144].

Responses of the cholinergic system, expressed as changes in levels of ACh in multiple brain areas, to aging and administration of tacrine, a well-established AChE inhibitor, were investigated in Paper II. Metabolism of ACh, and thus choline, is associated with multiple metabolic pathways, for instance phospholipid synthesis and lipid signaling. Therefore, an untargeted approach towards numerous CNS metabolic pathways was subsequently applied (Paper III). In addition, since the monoaminergic systems (DA, NE, and 5-HT) are regulated by cholinergic modulation and strong interconnections among several neurotransmitters and their metabolites have been detected (including for instance GABA and His), these systems were also investigated (Paper IV). These studies are described in more detail in the following sections.

## Quantification of ACh brain levels: age-related attenuation in the retrosplenial cortex in response to tacrine (Paper II)

The cholinergic system is an essential component of cognitive health and it is severely degenerated in AD and related dementias [92,145,146]. Therefore, as the neurotransmitter of the cholinergic system, ACh has received a notable scientific attention.

In Study II, a molecular specific MALDI-MSI approach was developed for the quantitative imaging of ACh in multiple brain areas of mice sampled at two ages, 12 weeks and 14 months (designated 12-w and 14-m, respectively), with and without the AChE inhibitor tacrine (designated tacrine and control, respectively).

MALDI-MSI analysis of ACh ( $m/z$  146.1176) in sagittal and coronal mouse brain sections demonstrated the neurotransmitter's presence in brain areas with major cholinergic neurons projecting to the forebrain and mid-brain (mesopontine nuclei), as well as locations of interneurons (Str) and areas that receive cholinergic innervation (cortical areas and Hip) (Figure 9).

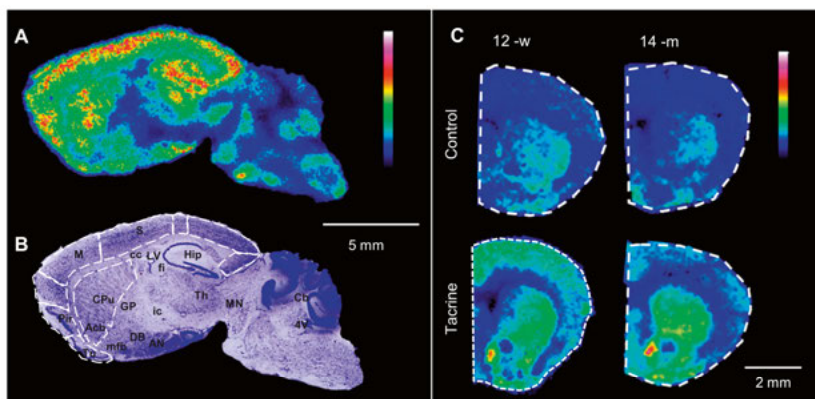


**Figure 9.** Brain distribution of ACh in sagittal and coronal mouse brain tissue sections. A) MALDI-MSI of ACh ( $m/z$  146.1176, scaled to 60% of max intensity and normalized to the internal standard) in a representative sagittal mouse brain section (lateral 1.7 mm) of a 14-m tacrine-administered animal at a lateral resolution of 60  $\mu\text{m}$ . B) The tissue section was subsequently washed and subjected to Nissl staining and brain regions of interest were annotated. C) MALDI-MSI of ACh in representative coronal brain sections (0.98 mm from bregma) from 12-w and 14-m controls and tacrine-administered animals (images scaled to 40% of max intensity). Abbreviations: Acb, nucleus accumbens; AN amygdalar nuclei, Cb, cerebellum; CPu, caudate putamen; DB, nucleus of diagonal band; GP, globus pallidus; M, motor cortex; MN, mesopontine nuclei; Pir, piriform cortex; SC, somatosensory cortex; Th, thalamus; Tu, olfactory tubercle; cc, corpus callosum; fi, fimbria of hippocampus; ic, internal capsule; mfb, medial forebrain bundle; LV, lateral ventricles; 4V, fourth ventricle.

Tacrine administration significantly increased the ACh levels in cortical areas, striatum (CPu and Acb), basal forebrain (medial septum nucleus and diagonal band, MSDB) and Hip (hippocampus proper and dentate gyrus), according to two-way ANOVA ( $P < 0.05$ ). Most importantly, a significant age-specific response to tacrine was detected in the retrosplenial cortex (RS). In this post-cingulate brain region, AChE inhibition led to higher ACh levels in 12-w than in 14-m mice (Figure 10), indicating that aged mice were less responsive than younger animals to tacrine in this area.

RS is a substantial transit region between the Hip and cingulate cortex (Cg), receiving cholinergic input from the MSDB [147,148]. It has been shown to play complementary roles with the Hip in cognitive function and spatial navigation [147]. The RS is reportedly one of the first brain regions to show pathological effects in early onset of AD and mild cognitive impairment [149-152]. It is, therefore, highly important to detect changes in cholinergic responsivity in this brain area in early stages of aging, as in Study II.

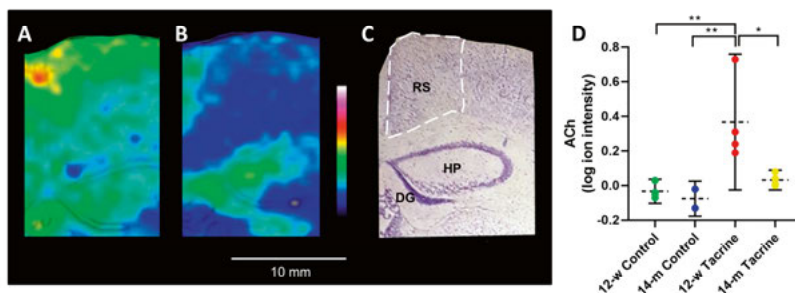


**Figure 10.** Age-related decrease of ACh concentration in RS in response to AChE inhibition. A, B) MALDI-MSI of ACh distribution in the RS of 12-w and 14-m tacrine-dosed animals (100  $\mu\text{m}$  lateral resolution, images scaled to 40% of max intensity), respectively. The MALDI-MS and Nissl stained images are overlaid using the image fusion function implemented in msIQuant software for better delineation of the brain structures. C) The tissue section was washed and subjected to Nissl staining; brain structures of interest are annotated. The RS is highlighted by white dashed lines. D) Dot plot of the log ion intensities of ACh in the RS between the different groups. Error bars show 95% confidence interval ( $n=4$ ). \* $P<0.05$ , \*\* $P<0.01$ . Abbreviations: DG, dentate gyrus; HP, hippocampal proper; RS, retrosplenial cortex.

No significant age-related differences in the ACh brain levels of control animals were observed in this study. Results of previous studies on the impact of normal aging on the cholinergic system have been conflicting, partially due to differences in experimental species, ages of the animals, and experimental procedures [93,121,153,154]. In addition, some studies indicate that cholinergic dysfunction is associated with pathological rather than normal aging [93,154].

ACh concentrations were measured in coronal brain sections. The average ACh concentrations in the investigated brain areas (Cx, CPu, and Hip) of 12-w control, 14-m control, 12-w tacrine and 14-m tacrine mice were 8.11 ( $\pm 1.40$ ), 7.80 ( $\pm 1.04$ ), 18.20 ( $\pm 5.34$ ), and 11.52 ( $\pm 3.00$ ) pmol/mg tissue, respectively.

Generally, the MALDI-MSI technique presented in Paper II provided robust measurements of ACh levels and distributions in mouse brain sections, together with new insights into effects of the AChE inhibitory drug tacrine and aging, especially in the RS area.

## Quantification of tacrine in mouse brain tissue sections: effects of aging on brain distribution (Paper II)

For the MALDI-MSI and quantification of tacrine, 9AA was selected as the internal standard due to its structural similarity to tacrine. Tacrine ( $m/z$  199.123) was widely distributed throughout the brain 30 min following its

administration, indicating high BBB transport [155,156], with similar localization in the grey matter in both 12-w and 14-m animals (Figure 11). Concentrations of tacrine in coronal mouse brain sections of tacrine-administered 12-w and 14-m mice were found to be very similar ( $6.21 \pm 0.34$  and  $6.02 \pm 0.57$  pmol/ mg tissue, respectively). In contrast, MSI of the hydroxylated tacrine metabolites [157,158] (1-OH-tacrine, 2-OH-tacrine and/or 4-OH-tacrine,  $m/z$  215.1178) in the same experiments showed that they were more abundant in the ventricular areas (lateral and fourth ventricles) and (especially) choroid plexus, than in grey and white matter areas, indicating lower rates of BBB transport. The brain abundance of OH-tacrine was significantly lower in the 14-m mice than in the younger animals ( $P < 0.05$ ). This may be associated to age-related reduction in drug-metabolizing enzyme activity, especially of the CYP1A2 isoform, which catalyzes transformation of tacrine to OH-tacrine [159].

This analysis highlighted MSI's potential utility for multimolecular detection and concomitant investigation of both neuroactive compounds and their molecular targets.

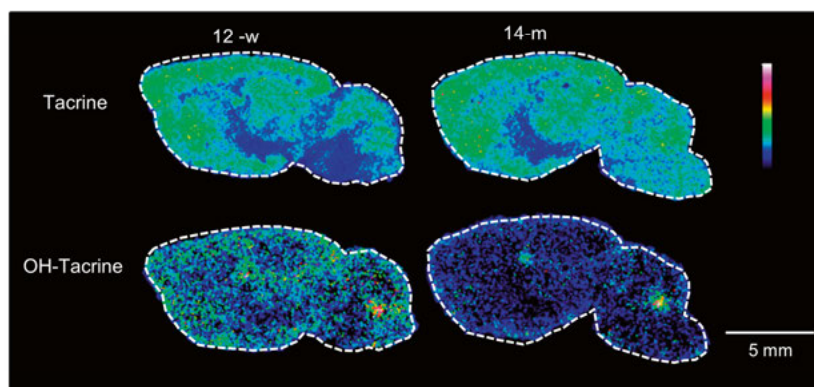


*Figure 11.* . Brain distribution of tacrine and its hydroxylated metabolites after i.p. administration (10 mg/kg). Sagittal brain tissue sections imaged by MALDI-MS showing tacrine ( $m/z$  199.123) in 12-w and 14-m mice, respectively (upper panels, 35% of max intensity). Sagittal brain tissue sections imaged by MALDI-MS showing OH-tacrine ( $m/z$  215.118) in 12-w and 14-m mice, respectively (lower panels, 20% of max intensity). Both analytes were imaged at a lateral resolution of  $80 \mu\text{m}$ .

### Age-induced metabolic alterations in the CNS (Paper III)

Paper III reports use of the combination of MALDI-FTICR-MSI and MVDA for identifying age-related CNS molecules in pools of thousands of compounds in multiple brain structures, such as Cx, RS, Hip, Str, cc, and medial forebrain bundle (mfb). The analysis was performed at relatively high lateral

and mass resolution, in a time-efficient manner. At the same time, effects of the AChE-inhibiting drug tacrine were also examined, in attempts to obtain comprehensive insights into the investigated CNS systems.

## Effects of aging and AChE inhibition by tacrine on acetylcholine and L-carnitine metabolism

As reported in Paper II, an age-dependent response of the cholinergic system was detected in the RS, with young (12-w) animals exhibiting significantly higher tacrine-induced elevation of ACh than older (14-m) animals. In Study III, further molecular alterations in the ACh metabolic pathway were detected. Specifically, cytidine 5'-diphosphocholine (CDP-choline) and L- $\alpha$ -glycerylphosphorylcholine ( $\alpha$ -GPC), intermediate molecules of the choline pathway that are abundant in the brain, were decreased by tacrine administration in all examined brain structures (Figure 12 A-C). Moreover,  $\alpha$ -GPC levels in the RS decreased in an age-dependent fashion, as the reduction was significantly stronger in 14-m animals than in the 12-w group.

Betaine, the final metabolite of choline metabolism, which has osmoprotective properties [160], was abundant in the thalamus and cerebellum and its levels were significantly elevated by aging and AChE inhibition in cortical areas and the Hip ( $P < 0.01$ ). Choline and its metabolic intermediates are not only vital precursors of the neurotransmitter ACh, they also play key roles in phospholipid synthesis and cell signaling. Thus, inhibiting AChE clearly has pleiotropic effects on cellular metabolism and neurotransmission.

The L-carnitine pathway is reportedly closely connected to ACh synthesis and metabolism, mainly through acetyl-L-carnitine's role as a potential acetyl donor [161]. L-carnitine was significantly elevated by aging (Figure 12 D) in control animals in the mfb and Str ( $P < 0.05$ ). RS was the only examined brain area where L-carnitine was significantly elevated by tacrine, particularly in the 14-m animals ( $P < 0.05$ ). Levels of acylcarnitines with both short fatty acid chains (acetyl-L-carnitine, propionyl-L-carnitine, butyryl-L-carnitine, hydroxybutyryl-L-carnitine, and glutaryl-L-carnitine) and long fatty acid chains (OH-undecanoyl-L-carnitine, palmitoyl-L-carnitine, and C-18-L-carnitine) were also elevated by aging, especially in the Str and Hip. However, in contrast to their precursor, a tacrine-induced decline in their levels was observed, especially in the mfb, as illustrated for acetyl-L-carnitine (Figure 12D). Age-induced elevation of L-carnitine and acylcarnitines can be considered an indicator of mitochondrial dysfunction, a key factor of cellular senescence.

Tacrine is reportedly a possible substrate of OCTN2 as it inhibits OCTN2-mediated uptake of L-carnitine and acetyl-L-carnitine [162,163]. Therefore, we examined *in vitro* whether effects of tacrine and 1-OH-tacrine on the carnitine pathway could be at least partially explained by their inter-

action with OCTN1 and OCTN2. Experiments showed that both tacrine and OH-tacrine significantly inhibited OCTN1/OCTN2-mediated uptake of quinidine (a known substrate of these transporters). Uptake experiments further showed that tacrine is a substrate of both OCTN transporters, whereas OH-tacrine is only a substrate of the OCTN1 transporter since uptake of both compounds was significantly reduced in the presence of the control inhibitor verapamil. It seems likely, therefore, that tacrine may interfere with the brain or cellular uptake transport mechanism of L-carnitine and acetyl-L-carnitine, leading to altered levels in the brain tissue.

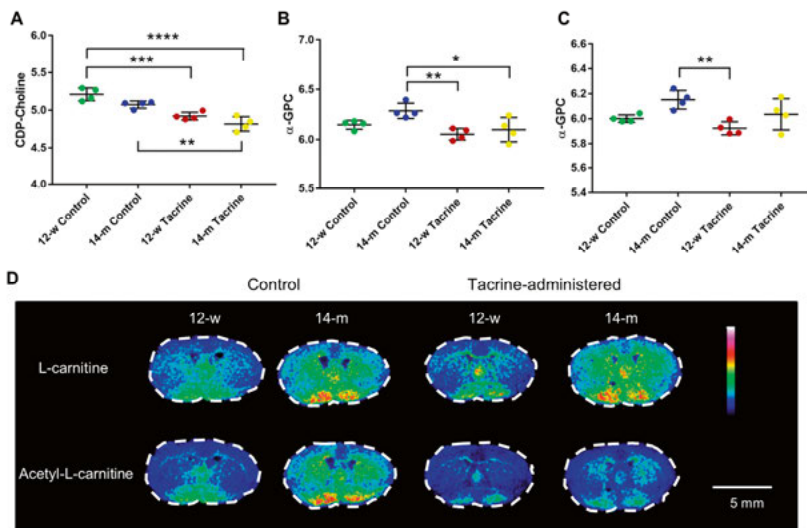


**Figure 12.** Effects of aging and tacrine administration in the ACh and L-carnitine pathways. A) Dot plot of the log ion intensities of CDP-choline in the Str of the different animal groups. B, C) Dot plots of the log ion intensities of α-GPC in the RS and Hip, respectively, of the different animal groups. Error bars show 95% confidence interval ( $n=4$ ). \* $P<0.05$ , \*\* $P<0.01$ , \*\*\* $P<0.001$ , \*\*\*\* $P<0.0001$ . D) MALDI-MSI of L-carnitine ( $m/z$  162.112) and acetyl-L-carnitine ( $m/z$  204.123) in coronal mouse brain tissue sections (0.26 mm from bregma) of 12-w and 14-m control and tacrine administered animals, at a lateral resolution of 100  $\mu\text{m}$ . The data are normalized to the RMS (images were scaled to 100% of maximum intensity).

## Age-induced increases in antioxidant and neuroprotective molecules

L-carnitine and acetyl-L-carnitine, brain levels of which increased with age, have been described as neuroprotective factors [161,164-168]. Importantly, however, other molecules with well-established antioxidant and geroprotective properties (carnosine and α-tocopherol), [169-171] also exhibited age-related elevation in the brain (Figure 13). We found that levels of the dipeptide carnosine (β-alanyl-L-histidine) and an analog, homocarnosine, in-

creased with age in all investigated brain areas.  $\alpha$ -tocopherol was significantly elevated in the hippocampal area of the older animals and exhibited age-induced elevation in the first and sixth cortical layers and Str. Since early aging was considered in this study, these findings may be related to a protective cellular response to elevated oxidative products connected to cellular damage. Tacrine administration did not seem to have any effect on levels of these molecules ( $P>0.2$ ).

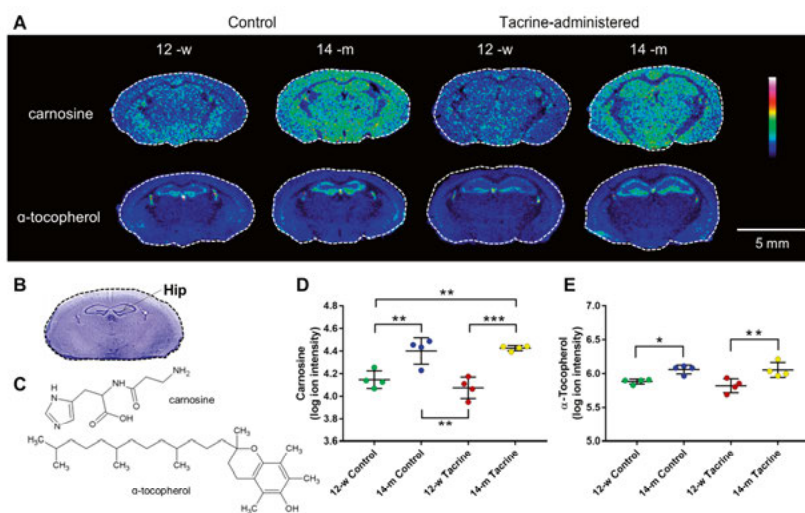


**Figure 13.** Effects of aging on the neuroprotective/antioxidant molecules carnosine and  $\alpha$ -tocopherol. A) MALDI-MSI of carnosine and  $\alpha$ -tocopherol in mouse brain tissue sections (-1.1 to -1.60 mm from bregma) from 12-w and 14-m control and tacrine administered animals at a lateral resolution of 80  $\mu$ m (scaled to 50% of maximum intensity). B) Example of a brain tissue section which was washed and stained with the Nissl method after MALDI-MSI. C) Chemical structures of carnosine and  $\alpha$ -tocopherol. D) Dot plot of log ion intensities of carnosine in Hip. E) Dot plot of log ion intensities of  $\alpha$ -tocopherol in Hip. Error bars show 95% confidence interval ( $n=4$ ). \* $P<0.05$ , \*\* $P<0.01$ , \*\*\* $P<0.001$ .

## Impact of age on brain lipids

Aging significantly affected lipids in all considered brain structures. Levels of certain phosphatidylcholine (PC) species were lower in 14-m animals, whereas levels of hexosylated (glucosylated and/or galactosylated) ceramides (HexCers), also known as cerebroside, were substantially higher than in the younger animals (Figure 14A, B). Sphingosine (d18:1), a ceramide precursor, was significantly lower in 14-m animals, confirming age-induced metabolic disturbances of this pathway (Figure 14 C).

These MSI data are important since lipid signaling is reportedly involved in cellular senescence and neurodegeneration [172,173]. Reductions in levels of PC species in plasma of AD patients have been reported, suggesting that

an increase in rates of phospholipase A2-mediated PC hydrolysis is the causative factor [173]. The significantly age-disrupted sphingolipid metabolism identified and imaged in Study III may serve as a valuable indicator of aging. Sphingolipids are bioactive lipids that play crucial roles in apoptotic processes and inflammation [174]. Elevated levels of ceramides (basic structural elements of all sphingolipids) and HexCers have been discovered in senescence rodent models and AD patient samples [172-175].

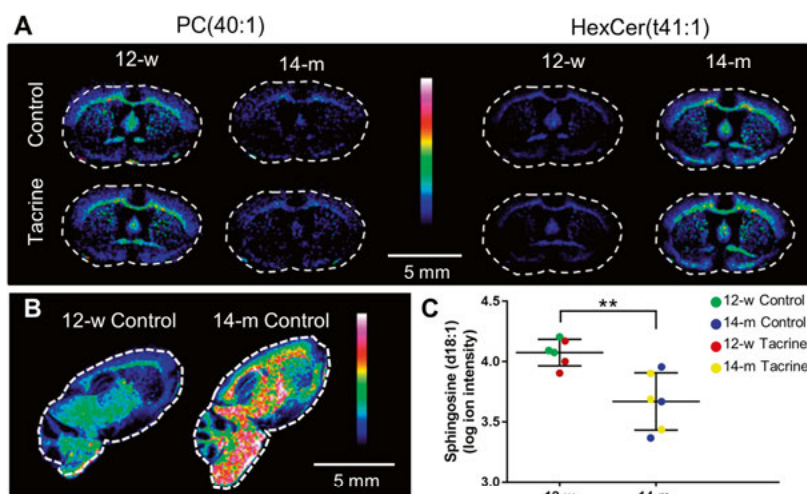


**Figure 14.** Effects of aging on brain lipid species. A) MALDI-MSI of PC(40:1) ( $m/z$  882.6309) and HexCer(t41:1) ( $m/z$  836.654) in coronal mouse brain tissue sections (0.26 mm from bregma) at a lateral resolution of 100  $\mu\text{m}$  (scaled to 100% of maximum intensity). B) MALDI-MSI of HexCer(t41:1) (scaled to 60% of maximum intensity) in sagittal control mouse brain tissue sections at a lateral resolution of 100  $\mu\text{m}$ . C) Dot plot of the log ion intensities of sphingosine (d18:1) extracted from whole sagittal mouse brain tissue sections derivatized with DPP-TFB. Error bars show 95% confidence interval ( $n=3$ ). \*\* $P<0.01$ .

In summary, MSI combined with MVDA analysis demonstrated metabolic disturbances, such as mitochondrial dysfunction and abnormal lipid signaling, which are strongly associated with aging. Observed age-associated increases in levels of multiple endogenous antioxidants suggest that mice of the studied ages may have compensatory mechanisms that mitigate cellular damage caused by these perturbations. The applied technology provided detailed insights into early stage mechanisms of normal brain aging, which are important for understanding the aging process.

## Aging effects on the catecholamine, serotonin, histamine and GABA neurotransmitter systems in the brain (Paper IV)

A recently developed derivatization method for the MSI of primary amines and phenols [33] was implemented in Study IV to investigate age-induced alterations in brain levels of DA, NE, 5-HT, GABA, His, and several of their metabolites.

MALDI-MSI of sagittal and coronal mouse brain tissue sections revealed strong localization of DA and its main CNS metabolites in the CPu, the input structure of the nigrostriatal dopaminergic pathway. DA levels were significantly lower in the ventral pallidum (PALv) ( $P < 0.05$ ) of the 14-m control animals than in 12-w controls (Figure 15A, B). However, no age-related difference in its levels was observed after tacrine administration. Levels of 3-methoxytyramine (3-MT), the DA metabolite formed by catalytic action of catechol-O-methyl transferase (COMT), were decreased by aging in the PALv, CPu, and bed nucleus of stria terminalis (BNST) ( $P < 0.05$ ) (Figure 15). A significant tacrine-induced decrease in 3-MT levels was detected in the CPu in animals of both ages ( $P < 0.01$ ) (Figure 15A, D). Interestingly, however, in the PALv tacrine only significantly reduced 3-MT levels ( $P < 0.01$ ) in the 12-w group (Figure 15A, C). Since 3-MT has been considered a marker for DA release [176], its age and tacrine-induced decrease may indicate a decline in dopaminergic transmission. Levels of 3,4-dihydroxyphenylacetaldehyde (DOPAL), the metabolite of DA formed by action of monoaminoxidase MAO-A/B, were significantly elevated in CPu in older animals of both treatment groups (Figure 15A, E). This finding may be related to previously reported age-induced elevation of the brain concentration of MAO-B, but not MAO-A [177]. Increases in DOPAL, as a product of an oxidation reaction occurring in the brain, can be considered an indicator of increased oxidative processes during aging, which may participate in a compensatory mechanism involving increases in levels of endogenous antioxidants suggested in Paper III.

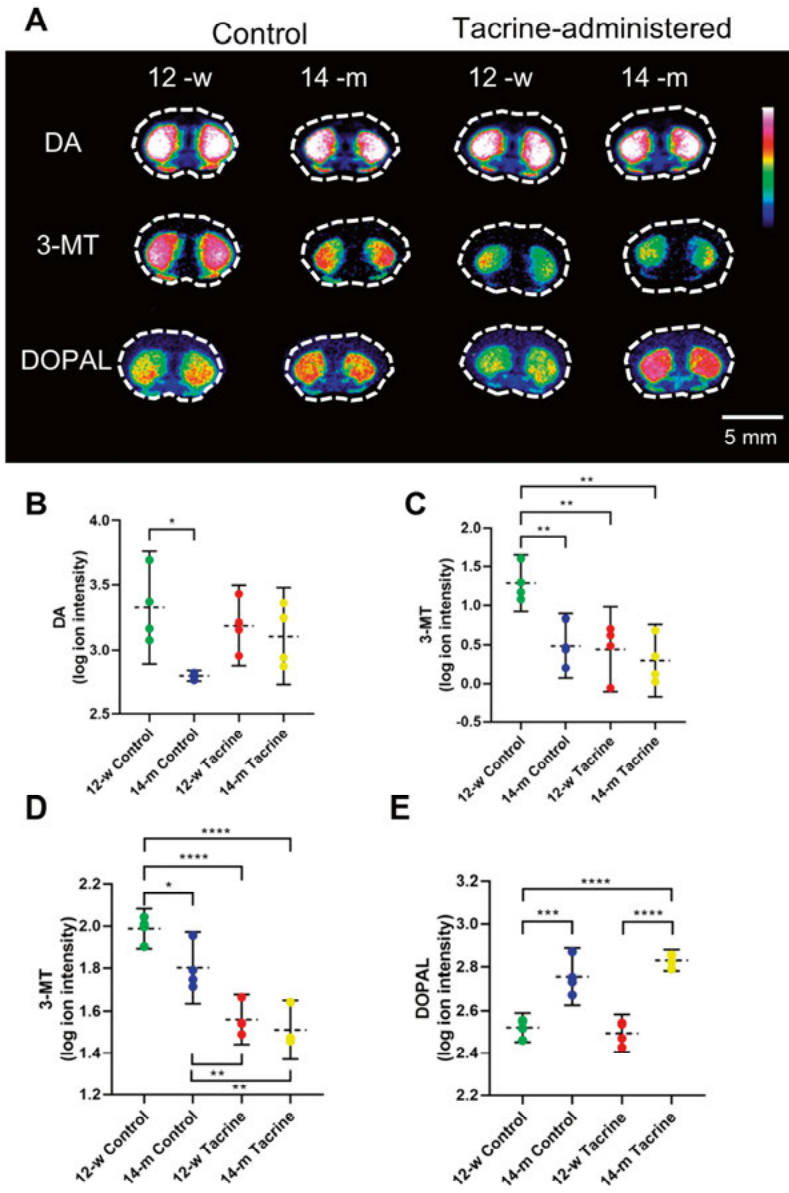


*Figure 15.* Effects of aging and tacrine administration on the dopaminergic metabolic pathway. A) MALDI-MSI of DA and its major brain metabolites 3-MT and DOPAL in coronal mouse brain tissue sections (0.26 mm from bregma) at a lateral resolution of 100  $\mu$ m (scaled to 60% of maximum intensity). B) Dot plot of log ion intensities of DA in the PALv. C, D) Dot plots of log ion intensities of 3-MT in the PALv and CPu, respectively. E) Dot plot of log ion intensities of DOPAL in the CPu. Error bars show 95% confidence interval ( $n=4$ ). \* $P<0.05$ , \*\* $P<0.01$ , \*\*\* $P<0.001$ , \*\*\*\* $P<0.0001$ .

Broader distributions in the brain and limited localization in the CPU were observed for NE and its major metabolites, 3,4-dihydroxyphenylglycol (DOPEG) and 3-methoxy-4-hydroxyphenylglycol (MOPEG). Higher NE levels in the somatosensory cortex (SC) and Hip were detected in 14-m mice of both treatment groups than in the corresponding younger animals ( $P < 0.05$ ), clearly indicating an age-dependent increase that was not affected by tacrine administration (Figure 16A-C). Interestingly, while no age-related differences in DOPEG levels were found in the control mice, levels of MOPEG, (a NE metabolite that is further downstream), were significantly lower in the BNST, PALv and Th of 14-m animals than in the 12-w group ( $P < 0.05$ ) (Figure 16 D-G), suggesting an age-associated decrease in NE turnover. Tacrine administration induced significant increases in levels of both metabolites in several NE-containing regions, such as the motor cortex (M), SC, and piriform, but significant reductions in NE levels in the SC and Hip.

In addition, DOPEG levels were higher in the Cg, SC, and M in 14-m tacrine administered animals than in the corresponding younger group ( $P < 0.09$ ). MOPEG levels were also significantly lower in the 14-m tacrine than in the 12-w tacrine group in the Th ( $P < 0.05$ ), but not in other areas such as the BNST and PALv, as observed in the control animals. These results indicate that AChE inhibition led to a significant increase in turnover of NE, which may be best explained by increased NE release from noradrenergic neurons [178,179].

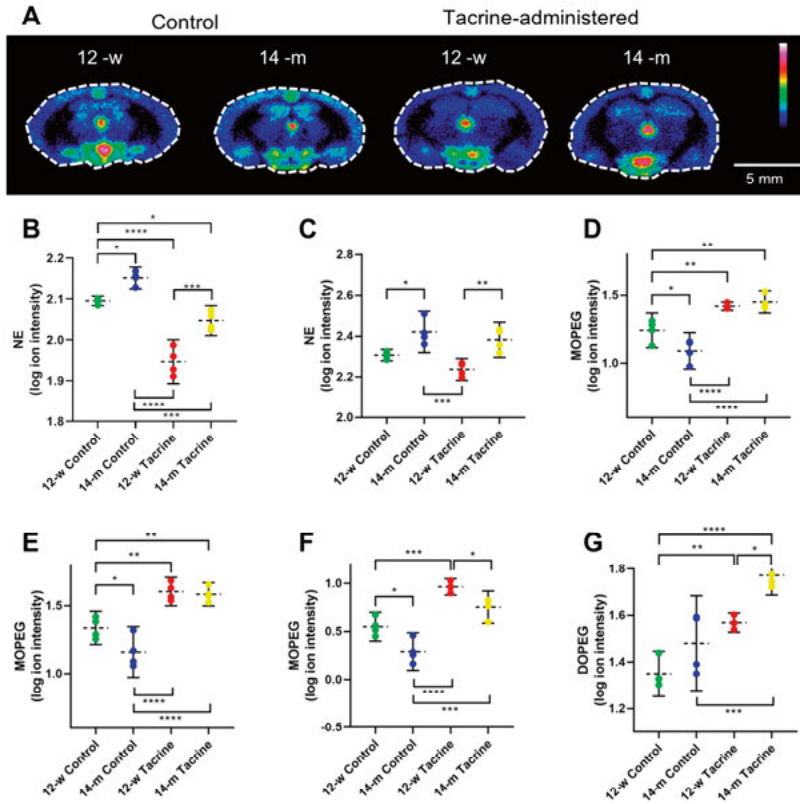


*Figure 16.* Effects of aging and tacrine administration on the noradrenergic metabolic pathway. A) MALDI-MSI of NE in coronal mouse brain tissue sections (-1.06 mm to -1.60 mm from bregma) at a lateral resolution of  $80\ \mu\text{m}$  (scaled to 40% of maximum intensity). B, C) Dot plots of the log ion intensities of NE in the Hip and S, respectively. D, E, F) Dot plots of log ion intensities of MOPEG in the PALV, BNST and Th, respectively. G) Dot plot of log ion intensity of DOPEG in the S. Error bars show 95% confidence interval ( $n=4$ ). \* $P<0.05$ , \*\* $P<0.01$ , \*\*\* $P<0.001$ , \*\*\*\* $P<0.0001$ .

In accordance with previous reports [180] 5-HT was localized in the PALV, Tu, BNST, lateral septum, Hyp, insular cortex, and ventral part of the CPU. In the control animals, 5-HT was significantly decreased by age ( $P<0.05$ ) in the Th, but no age-related difference in its levels was observed after tacrine administration (Figure 17).

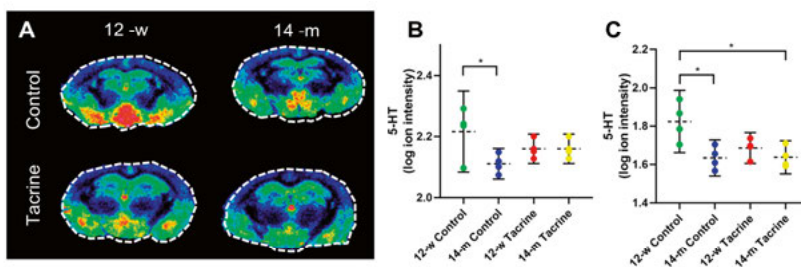


*Figure 17.* Effects of aging and tacrine administration on 5-HT. A) MALDI-MSI of 5-HT in coronal mouse brain tissue sections (-1.06 mm to -1.60 mm from bregma) at a lateral resolution of 80  $\mu\text{m}$  (scaled to 50% of maximum intensity). B, C) Dot plots of log ion intensities of 5-HT in the Amy and Th, respectively. Error bars show 95% confidence interval ( $n=4$ ). \* $P<0.05$ , \*\* $P<0.01$ .

His was localized mainly in the Hyp, BNST, PALv, Tu, and LS, but was less abundant in the CPu and cortex area [181]. No age-related differences in His levels between the 12-w and 14-m control groups were detected. However, after tacrine treatment, they were significantly higher in the Cg, CPu, and PALv ( $P<0.05$ ) in the older animals than in the younger animals. This indicates an age-related response of the histaminergic system to tacrine, possibly connected to previously reported age-related reductions in activity of histamine-n-methyl transferase, the major His metabolizing enzyme, which has also been identified as a tacrine target [182]. It should also be noted that no significant alterations were observed in the GABAergic system.

To summarize, in Study IV normal aging-induced modifications in the DA metabolic pathway were detected, mainly in the PALv and CPu, which are mainly innervated from the mesolimbic and nigrostriatal pathways, respectively [97,183]. These findings have possible implications for the reward and motor system. Age-related changes in the NE pathway were detected in the Hip, a brain area strongly associated with cognitive performance [184]. Age-dependent effects of AChE inhibition were especially detected in the PALv, a structure containing cholinergic neurons and involved in reward-related responses [89,103].

## Conclusions

In the studies this thesis is based, a comprehensive approach to improve understanding of critical issues in neuropharmacology was attempted by applying MSI technology. Complementary advantages of, and recent developments in, the two most widely applied MSI techniques in quantitative tissue distribution studies, MALDI and DESI, were exploited. Brain transport of pharmaceutical agents, a “bottleneck” in CNS drug development, was one of the foci. Roles of both passive diffusion and transport-mediated efflux in distributions of two drugs in the brain were demonstrated visually and quantitatively. Use of a MDR1 substrate drug with limited brain entrance (loperamide) aided illustration of the differences between uptake in the brain parenchyma and specific localization in the choroidal epithelium. Phenomena even in small structures like the choroid plexus were well illustrated by the combination of DESI and MALDI-MSI. However, further improvements of the lateral resolution of DESI-MSI could enhance understanding of the impact of MDR1-mediated transport in this area. Future applications of the technique in BBB studies would benefit from simultaneous quantitative MSI analysis of plasma samples for measuring brain to plasma ratios ( $K_p$ ).

Drug-target interactions in the CNS, specifically tacrine-induced AChE inhibition, were investigated by MALDI-MSI. The technique enabled detection of a “cascade” of neurochemical alterations induced by the drug in multiple brain areas, including changes in levels and distributions of not only neurotransmitters (ACh, DA metabolites, and NE) but also metabolic intermediates (e.g., CDP-choline) that had not been previously reported. Additional insights into the mechanisms involved, e.g., multi-target binding of the drug per se or ACh-induced alterations, could be obtained using a complementary approach, such as cholinergic receptor binding analysis.

Importantly, MSI allowed investigation of age-induced alterations in the CNS. Several region-specific metabolic and neurotransmitter changes were detected between brains of mice of two representative ages. Including samples of other ages could improve understanding of the underlying mechanisms in future studies. The analysis described here involved both targeted and untargeted approaches, showing the high potential of the technology for combination with robust statistical tools like MVDA techniques. In the presented studies, projection-based dimensional reduction methods (PCA and PLS-DA) were used to analyze large MALDI-MSI datasets, successfully

providing insights into multiple CNS systems modified by age in numerous brain areas. This approach assisted discrimination of experimental noise from biologically relevant information and showed the relative contributions of specific systems and brain structures in the detected age-related differences. Advanced multiway-decomposition methods, expanding PCA capacities could also be applied, while the data processing process could be further automated by building complete software packages providing pre-processing, data analysis, and evaluation in one platform. In addition, further instrumental advances combining high lateral and high mass resolution in a time-efficient manner would be highly valuable.

In summary, this thesis demonstrates:

- The potential utility of MSI in BBB transport studies, particularly DDIs involving MDR1 inhibition;
- Brain pharmacodynamic phenomena, with the simultaneous imaging of drug and endogenous molecular target distributions;
- Age-specific cholinergic responses in the RS, an enigmatic cortical area of increasing interest that is involved in important cognitive functions;
- Mitochondrial alterations induced by aging, expressed as perturbations of the L-carnitine metabolic pathway, especially in the Hip and Str;
- Region-specific changes in neurotransmitter release and metabolism triggered by aging;
- Age-dependent responses of several endogenous neurotransmitters and metabolites, e.g., 3-MT and His, to AChE inhibition.

# Populärvetenskaplig sammanfattning

Avbildande masspektrometri (MSI) är en analysteknik som möjliggör kartläggning av en stor mängd molekyler i biologiska vävnadssnitt samtidigt, till exempel i hjärnan. Flera olika sorts substanser och kroppsegna ämnen kan detekteras och avbildas, såsom läkemedel, neurotransmittorer, lipider, peptider och små proteiner. Matrix-assisted laser desorption ionization (MALDI) och desorption electrospray ionization (DESI) är de mest tillämpade MSI-teknikerna. Båda teknikerna kräver relativt enkla provupparbetningar. Kraftfulla MSI-instrument med hög massnoggrannhet, massupplösning och lateral upplösning ( $>5 \mu\text{m}$ ) kan kvantifiera och identifiera olika ämnen på ett snitt av en hjärna. Tekniken kan generera mycket stora datamängder som hanteras med snabba och kraftfulla mjukvaror.

I föreliggande avhandling används MSI för att adressera utmanande problem inom området neurofarmakologi. Läkemedel som är aktiva i centrala nervsystemet är extra svåra att utveckla på grund av att många av dem har svårt att passera genom blodhjärnbarriären. Att samtidigt undersöka distribution och koncentration av ett läkemedel i hjärnan och dess potentiella effekter på flera signalvägar i olika hjärnregioner är därför av stor betydelse för att förstå hur ett läkemedel fungerar.

I den första delen av avhandlingen så används MSI för att studera olika läkemedels förmåga att passera blodhjärnbarriären. I blodhjärnbarriären finns det specifika transportproteiner, exempelvis MDR1, som pumpar ut främmande ämnen från hjärnan för att skydda den. Ett av de studerade läkemedlen, loperamid, är substrat för MDR1 transportören. Med MSI analys påvisades en begränsad distribution till hjärnan av loperamid. Läkemedlet avbildades framförallt i choroid plexus, en hjärnregion som producerar cerebrospinalvätska. Koncentrationen av loperamid i hjärnan kunde dock ökas betydligt genom att samtidigt administrera ett läkemedel som fungerar som MDR1-hämmare. Med MALDI- och DESI-teknikerna kunde läkemedlen samtidigt avbildas i de olika experimenten och resultaten visar att MSI är ett nytt och viktigt verktyg för att studera interaktioner mellan läkemedel och deras upptag i hjärnan.

I den andra delen av avhandlingen så utnyttjades MSI tekniken för undersökning av farmakodynamiska läkemedelsaspekter, med fokus på hämning av acetylkolinesteras (enzymet som bryter ner acetylkolin) och hur dess effekter påverkas av normalt åldrande. MSI analyser visar att effekten av acetylkolinesterasinhäring minskar signifikant med ålder i ett litet område i

hjärnbarken (retrosplenial cortex). Hjärnregionen har stor betydelse vid inlärning och navigering. Genom att använda multivariata dataanalyser påvisades förändringar av flera metaboliska vägar i specifika hjärnområden som beror på normalt åldrande. Förändringar av mitokondriell funktion, fettsyra-signalering och acetylkolinmetabolism påvisades. Dessutom upptäcktes åldersberoendenivåförändringar av monoaminerga neurotransmittorer och deras metaboliter, särskilt i hjärnområden som ventrala pallidum, caudatus-putamen, hippocampus och kortikala understrukturer. Även acetylkolinesterashämning inducerade ålders- och regionsspecifika förändringar på neurotransmittorsystemen.

Sammanfattningsvis så visar studierna i avhandlingen hur MALDI- och DESI-MSI teknologin kan användas för att utföra omfattande och avancerade farmakokinetiska och farmakodynamiska studier i hjärnan.

# Acknowledgements

The studies presented in this thesis were performed at the Department of Pharmaceutical Biosciences, Faculty of Pharmacy, Uppsala University, Sweden.

The work was financially supported by ARIADME, a European Community's Seventh Framework Program (FP7 ITN, under Grant Agreement No. 607517), the Swedish Research Council (Medicine and Health, grant no. 2018-03320, Natural and Engineering Science, grant no. 2018-05501), the Swedish Brain Foundation (no. FO2018-0292), the Swedish Foundation for Strategic Research (grant no. RIF14-0078), and the Science for Life Laboratory. Travel grants for presenting my work at international conferences were also provided by Apotekarsocieteten.

I would like to express my gratitude to the following people.

First of all, I would like to thank my supervisor, Prof. Per Andrén for giving me the opportunity to participate in the exciting research conducted in his group, supporting and encouraging new ideas, being always kind and understanding and a great educator. Tack så mycket!

I would like to thank my co-supervisors, Reza Shariatgorji, Anna Nilsson, Maria Karlgren and Irena Loryan for the support, the enthusiasm, the kindness, the ideas, the great and didactic discussions and the fruitful and nice time we spent together. Thank you!! Reza, you have also been the most intellectual, educational and kind office-mate!

I would like to thank Prof. Per Svenningsson and his group in Karolinska Institute, and especially Marcela Pereira, Xiaoqun Zhang and Ioannis Mantas for the wonderful collaboration.

I would also like to thank Richard Goodwin, Nicole Strittmatter, Gregory Hamm, John Swales and Christopher Hardy for the excellent collaboration in AstraZeneca in Cambridge, UK.

I am very grateful and happy for having met and worked with all the members of the group, current and previous, and I sincerely thank all of you: Per, Anna, Reza, Patrik, Henrik L., Henrik W., Elva, Heather, Dominika, Erik and Friederike. Thank you for your help and nice collaboration! I would also like to thank the guest researchers and students who have worked in the lab, Jinrui, Lingjie, Florian, Michael, Asdis, Nuria and Halla.

Elva and Heather, you are such great friends and I am so glad I met you!  
Elva, σε ευχαριστώ τόσο πολύ για την αμέριστη συμπαράσταση, είσαι για μένα οικογένεια, besti vinur!

I would like to thank all people from B5:2 corridor for being so kind and making a nice working environment. I would also like to thank all the administrators of the department for their valuable help, as well as Lena Norgren and Magnus Efverström. I would also like to thank the Head of Department, Prof. Björn Hellman.

I would also like to thank Prof. Margareta Hammarlund-Udenaes for the nice collaboration.

Khadijah, thank you for being a nice friend and always kind!

Andrea, you are my complementary twin, the voice of logic, always calming down my stress. I wouldn't imagine life in Uppsala without you!

I would like to thank my former supervisor, Prof. Anna Tsantili. Κυρία Άννα, σας ευχαριστώ για όλα!

Thank you, my big lovely greek family! My mom and dad, Maria and Stavros, my grandmothers, Ioanna and Theodosia, my grandfathers, Panagiotis and Giorgos, my aunt and uncle Aggeliki and Nikos, δεν υπάρχουν λόγια να εκφράσω την ευγνωμοσύνη μου για την αγάπη και την υποστήριξη όλα αυτά τα χρόνια! Thank you Panagiotis for making the cover of this thesis and for being the best little brother ever!

Lefteris, your support was amazing. Σ'ευχαριστώ που υπάρχεις!!

# References

1. Collaborators GBDN (2019) Global, regional, and national burden of neurological disorders, 1990-2016: a systematic analysis for the Global Burden of Disease Study 2016. *Lancet Neurol* 18: 459-480.
2. Choi DW, Armitage R, Brady LS, Coetzee T, Fisher W, et al. (2014) Medicines for the mind: policy-based "pull" incentives for creating breakthrough CNS drugs. *Neuron* 84: 554-563.
3. Kola I, Landis J (2004) Can the pharmaceutical industry reduce attrition rates? *Nat Rev Drug Discov* 3: 711-715.
4. Pardridge WM (2005) The blood-brain barrier: bottleneck in brain drug development. *NeuroRx* 2: 3-14.
5. Kesselheim AS, Hwang TJ, Franklin JM (2015) Two decades of new drug development for central nervous system disorders. *Nat Rev Drug Discov* 14: 815-816.
6. Caprioli RM, Farmer TB, Gile J (1997) Molecular imaging of biological samples: localization of peptides and proteins using MALDI-TOF MS. *Anal Chem* 69: 4751-4760.
7. Nilsson A, Goodwin RJ, Shariatgorji M, Vallianatou T, Webborn PJ, et al. (2015) Mass spectrometry imaging in drug development. *Anal Chem* 87: 1437-1455.
8. Shariatgorji M, Svenningsson P, Andren PE (2014) Mass Spectrometry Imaging, an Emerging Technology in Neuropsychopharmacology. *Neuropsychopharmacology* 39: 34-49.
9. Vismeh R, Waldon DJ, Teffera Y, Zhao ZY (2012) Localization and Quantification of Drugs in Animal Tissues by Use of Desorption Electrospray Ionization Mass Spectrometry Imaging. *Analytical Chemistry* 84: 5439-5445.
10. Rubakhin SS, Jurchen JC, Monroe EB, Sweedler JV (2005) Imaging mass spectrometry: fundamentals and applications to drug discovery. *Drug Discov Today* 10: 823-837.
11. Shariatgorji M, Nilsson A, Goodwin RJ, Kallback P, Schintu N, et al. (2014) Direct targeted quantitative molecular imaging of neurotransmitters in brain tissue sections. *Neuron* 84: 697-707.
12. Shariatgorji M, Nilsson A, Goodwin RJA, Svenningsson P, Schintu N, et al. (2012) Deuterated Matrix-Assisted Laser Desorption Ionization Matrix Uncovers Masked Mass Spectrometry Imaging Signals of Small Molecules. *Analytical Chemistry* 84: 7152-7157.
13. Shariatgorji M, Nilsson A, Kallback P, Karlsson O, Zhang XQ, et al. (2015) Pyrylium Salts as Reactive Matrices for MALDI-MS Imaging of Biologically Active Primary Amines. *Journal of the American Society for Mass Spectrometry* 26: 934-939.
14. Shariatgorji M, Strittmatter N, Nilsson A, Kallback P, Alvarsson A, et al. (2016) Simultaneous imaging of multiple neurotransmitters and neuroactive substances in the brain by desorption electrospray ionization mass spectrometry. *Neuroimage* 136: 129-138.

15. Liu XH, Ide JL, Norton I, Marchionni MA, Ebling MC, et al. (2013) Molecular imaging of drug transit through the blood-brain barrier with MALDI mass spectrometry imaging. *Scientific Reports* 3.
16. Randall EC, Emdal KB, Laramy JK, Kim M, Roos A, et al. (2018) Integrated mapping of pharmacokinetics and pharmacodynamics in a patient-derived xenograft model of glioblastoma. *Nat Commun* 9: 4904.
17. Kertesz V, Van Berkel GJ, Vavrek M, Koeplinger KA, Schneider BB, et al. (2008) Comparison of drug distribution images from whole-body thin tissue sections obtained using desorption electrospray ionization tandem mass spectrometry and autoradiography. *Anal Chem* 80: 5168-5177.
18. Karas M, Hillenkamp F (1988) Laser desorption ionization of proteins with molecular masses exceeding 10,000 daltons. *Anal Chem* 60: 2299-2301.
19. Mochizuki T, Mima K, Ikeda N, Kodama R, Shiraga H, et al. (1987) Experimental evidence of ionization burnthrough and absorption resonance in radiative energy transport in hot dense matter. *Phys Rev A Gen Phys* 36: 3279-3287.
20. Clark AE, Kaleta EJ, Arora A, Wolk DM (2013) Matrix-assisted laser desorption ionization-time of flight mass spectrometry: a fundamental shift in the routine practice of clinical microbiology. *Clin Microbiol Rev* 26: 547-603.
21. Khatib-Shahidi S, Andersson M, Herman JL, Gillespie TA, Caprioli RM (2006) Direct molecular analysis of whole-body animal tissue sections by imaging MALDI mass spectrometry. *Anal Chem* 78: 6448-6456.
22. Carlred L, Michno W, Kaya I, Sjoval P, Syvanen S, et al. (2016) Probing amyloid-beta pathology in transgenic Alzheimer's disease (tgArcSwe) mice using MALDI imaging mass spectrometry. *J Neurochem* 138: 469-478.
23. Seeley EH, Schwamborn K, Caprioli RM (2011) Imaging of intact tissue sections: moving beyond the microscope. *J Biol Chem* 286: 25459-25466.
24. Stoekli M, Chaurand P, Hallahan DE, Caprioli RM (2001) Imaging mass spectrometry: a new technology for the analysis of protein expression in mammalian tissues. *Nat Med* 7: 493-496.
25. Deutskens F, Yang J, Caprioli RM (2011) High spatial resolution imaging mass spectrometry and classical histology on a single tissue section. *J Mass Spectrom* 46: 568-571.
26. Kompauer M, Heiles S, Spengler B (2017) Atmospheric pressure MALDI mass spectrometry imaging of tissues and cells at 1.4- $\mu$  m lateral resolution. *Nature Methods* 14: 90-96.
27. Takats Z, Wiseman JM, Gologan B, Cooks RG (2004) Mass spectrometry sampling under ambient conditions with desorption electrospray ionization. *Science* 306: 471-473.
28. Campbell DI, Ferreira CR, Eberlin LS, Cooks RG (2012) Improved spatial resolution in the imaging of biological tissue using desorption electrospray ionization. *Anal Bioanal Chem* 404: 389-398.
29. Tillner J, Wu V, Jones EA, Pringle SD, Karancsi T, et al. (2017) Faster, More Reproducible DESI-MS for Biological Tissue Imaging. *J Am Soc Mass Spectrom* 28: 2090-2098.
30. Michalski A, Damoc E, Hauschild JP, Lange O, Wiegand A, et al. (2011) Mass spectrometry-based proteomics using Q Exactive, a high-performance benchtop quadrupole Orbitrap mass spectrometer. *Mol Cell Proteomics* 10: M111 011015.
31. Comisarow MB, Marshall AG (1996) The early development of Fourier transform ion cyclotron resonance (FT-ICR) spectroscopy. *J Mass Spectrom* 31: 581-585.

32. Puolitaival SM, Burnum KE, Cornett DS, Caprioli RM (2008) Solvent-free matrix dry-coating for MALDI imaging of phospholipids. *J Am Soc Mass Spectrom* 19: 882-886.
33. Shariatgorji M, Nilsson A, Fridjonsdottir E, Vallianatou T, Katan T, et al. (2019) Comprehensive mapping of neurotransmitter networks by MALDI-MS imaging. *Nat Methods*, accepted for publication
34. Jones EA, Deininger SO, Hogendoorn PCW, Deelder AM, McDonnell LA (2012) Imaging mass spectrometry statistical analysis. *J Proteomics* 75: 4962-4989.
35. Kallback P, Nilsson A, Shariatgorji M, Andren PE (2016) msIQuant--Quantitation Software for Mass Spectrometry Imaging Enabling Fast Access, Visualization, and Analysis of Large Data Sets. *Anal Chem* 88: 4346-4353.
36. Kallback P, Shariatgorji M, Nilsson A, Andren PE (2012) Novel mass spectrometry imaging software assisting labeled normalization and quantitation of drugs and neuropeptides directly in tissue sections. *Journal of Proteomics* 75: 4941-4951.
37. Bemis KD, Harry A, Eberlin LS, Ferreira C, van de Ven SM, et al. (2015) Cardinal: an R package for statistical analysis of mass spectrometry-based imaging experiments. *Bioinformatics* 31: 2418-2420.
38. Nilsson A, Fehniger TE, Gustavsson L, Andersson M, Kenne K, et al. (2010) Fine mapping the spatial distribution and concentration of unlabeled drugs within tissue micro-compartments using imaging mass spectrometry. *PLoS One* 5: e11411.
39. Porta T, Lesur A, Varesio E, Hopfgartner G (2015) Quantification in MALDI-MS imaging: what can we learn from MALDI-selected reaction monitoring and what can we expect for imaging? *Anal Bioanal Chem* 407: 2177-2187.
40. Chumbley CW, Reyzer ML, Allen JL, Marriner GA, Via LE, et al. (2016) Absolute Quantitative MALDI Imaging Mass Spectrometry: A Case of Rifampicin in Liver Tissues (vol 88, pg 2392, 2016). *Analytical Chemistry* 88: 8920-8920.
41. Alexandrov T (2012) MALDI imaging mass spectrometry: statistical data analysis and current computational challenges. *BMC Bioinformatics* 13 Suppl 16: S11.
42. Dill AL, Eberlin LS, Zheng C, Costa AB, Ifa DR, et al. (2010) Multivariate statistical differentiation of renal cell carcinomas based on lipidomic analysis by ambient ionization imaging mass spectrometry. *Anal Bioanal Chem* 398: 2969-2978.
43. Jones EA, van Remoortere A, van Zeijl RJ, Hogendoorn PC, Bovee JV, et al. (2011) Multiple statistical analysis techniques corroborate intratumor heterogeneity in imaging mass spectrometry datasets of myxofibrosarcoma. *PLoS One* 6: e24913.
44. Dexter A, Race AM, Styles IB, Bunch J (2016) Testing for Multivariate Normality in Mass Spectrometry Imaging Data: A Robust Statistical Approach for Clustering Evaluation and the Generation of Synthetic Mass Spectrometry Imaging Data Sets. *Anal Chem* 88: 10893-10899.
45. Belaz KR, Tata A, Franca MR, Santos da Silva MI, Vendramini PH, et al. (2016) Phospholipid Profile and Distribution in the Receptive Oviduct and Uterus During Early Diestrus in Cattle. *Biol Reprod* 95: 127.
46. Amigo JM, Ravn C, Gallagher NB, Bro R (2009) A comparison of a common approach to partial least squares-discriminant analysis and classical least squares in hyperspectral imaging. *Int J Pharm* 373: 179-182.
47. Bro R, Kjeldahl K, Smilde AK, Kiers HA (2008) Cross-validation of component models: a critical look at current methods. *Anal Bioanal Chem* 390: 1241-1251.

48. Abraham G, Inouye M (2014) Fast principal component analysis of large-scale genome-wide data. *PLoS One* 9: e93766.
49. Verhoeckx KC, Bijlsma S, de Groene EM, Witkamp RF, van der Greef J, et al. (2004) A combination of proteomics, principal component analysis and transcriptomics is a powerful tool for the identification of biomarkers for macrophage maturation in the U937 cell line. *Proteomics* 4: 1014-1028.
50. Worley B, Powers R (2013) Multivariate Analysis in Metabolomics. *Curr Metabolomics* 1: 92-107.
51. Szymanska E, Saccenti E, Smilde AK, Westerhuis JA (2012) Double-check: validation of diagnostic statistics for PLS-DA models in metabolomics studies. *Metabolomics* 8: 3-16.
52. Worley B, Powers R (2016) PCA as a practical indicator of OPLS-DA model reliability. *Curr Metabolomics* 4: 97-103.
53. Pardridge WM (2012) Drug transport across the blood-brain barrier. *J Cereb Blood Flow Metab* 32: 1959-1972.
54. Abbott NJ, Patabendige AAK, Dolman DEM, Yusof SR, Begley DJ (2010) Structure and function of the blood-brain barrier. *Neurobiology of Disease* 37: 13-25.
55. Mathiisen TM, Lehre KP, Danbolt NC, Ottersen OP (2010) The perivascular astroglial sheath provides a complete covering of the brain microvessels: an electron microscopic 3D reconstruction. *Glia* 58: 1094-1103.
56. Eyal S, Hsiao P, Unadkat JD (2009) Drug interactions at the blood-brain barrier: Fact or fantasy? *Pharmacology & Therapeutics* 123: 80-104.
57. Broccatelli F, Larregieu CA, Cruciani G, Oprea TI, Benet LZ (2012) Improving the prediction of the brain disposition for orally administered drugs using BDDCS. *Adv Drug Deliv Rev* 64: 95-109.
58. International Transporter C, Giacomini KM, Huang SM, Tweedie DJ, Benet LZ, et al. (2010) Membrane transporters in drug development. *Nat Rev Drug Discov* 9: 215-236.
59. Tweedie D, Polli JW, Berglund EG, Huang SM, Zhang L, et al. (2013) Transporter studies in drug development: experience to date and follow-up on decision trees from the International Transporter Consortium. *Clin Pharmacol Ther* 94: 113-125.
60. Pochini L, Galluccio M, Scalise M, Console L, Indiveri C (2019) OCTN: A Small Transporter Subfamily with Great Relevance to Human Pathophysiology, Drug Discovery, and Diagnostics. *SLAS Discov* 24: 89-110.
61. del Amo EM, Urtti A, Yliperttula M (2008) Pharmacokinetic role of L-type amino acid transporters LAT1 and LAT2. *Eur J Pharm Sci* 35: 161-174.
62. Ghosh C, Gonzalez-Martinez J, Hossain M, Cucullo L, Fazio V, et al. (2010) Pattern of P450 expression at the human blood-brain barrier: roles of epileptic condition and laminar flow. *Epilepsia* 51: 1408-1417.
63. Damkier HH, Brown PD, Praetorius J (2013) Cerebrospinal fluid secretion by the choroid plexus. *Physiol Rev* 93: 1847-1892.
64. Saunders NR, Daneman R, Dziegielewska KM, Liddelow SA (2013) Transporters of the blood-brain and blood-CSF interfaces in development and in the adult. *Mol Aspects Med* 34: 742-752.
65. Spector R, Keep RF, Robert Snodgrass S, Smith QR, Johanson CE (2015) A balanced view of choroid plexus structure and function: Focus on adult humans. *Exp Neurol* 267: 78-86.
66. Strazielle N, Ghersi-Egea JF (2013) Physiology of blood-brain interfaces in relation to brain disposition of small compounds and macromolecules. *Mol Pharm* 10: 1473-1491.

67. Kodaira H, Kusuvara H, Fujita T, Ushiki J, Fuse E, et al. (2011) Quantitative Evaluation of the Impact of Active Efflux by P-Glycoprotein and Breast Cancer Resistance Protein at the Blood-Brain Barrier on the Predictability of the Unbound Concentrations of Drugs in the Brain Using Cerebrospinal Fluid Concentration as a Surrogate. *Journal of Pharmacology and Experimental Therapeutics* 339: 935-944.
68. Friden M, Bergstrom F, Wan H, Rehngrén M, Ahlin G, et al. (2011) Measurement of Unbound Drug Exposure in Brain: Modeling of pH Partitioning Explains Diverging Results between the Brain Slice and Brain Homogenate Methods. *Drug Metabolism and Disposition* 39: 353-362.
69. Hammarlund-Udenaes M, Friden M, Syvanen S, Gupta A (2008) On the rate and extent of drug delivery to the brain. *Pharm Res* 25: 1737-1750.
70. Loryan I, Sinha V, Mackie C, Van Peer A, Drinkenburg W, et al. (2014) Mechanistic understanding of brain drug disposition to optimize the selection of potential neurotherapeutics in drug discovery. *Pharm Res* 31: 2203-2219.
71. Friden M, Ducrozet F, Middleton B, Antonsson M, Bredberg U, et al. (2009) Development of a high-throughput brain slice method for studying drug distribution in the central nervous system. *Drug Metab Dispos* 37: 1226-1233.
72. Desai M, Slusarczyk AL, Chapin A, Barch M, Jasanoff A (2016) Molecular imaging with engineered physiology. *Nat Commun* 7: 13607.
73. Goodwin RJ, Mackay CL, Nilsson A, Harrison DJ, Farde L, et al. (2011) Qualitative and quantitative MALDI imaging of the positron emission tomography ligands raclopride (a D2 dopamine antagonist) and SCH 23390 (a D1 dopamine antagonist) in rat brain tissue sections using a solvent-free dry matrix application method. *Anal Chem* 83: 9694-9701.
74. Helms HC, Abbott NJ, Burek M, Cecchelli R, Couraud PO, et al. (2016) In vitro models of the blood-brain barrier: An overview of commonly used brain endothelial cell culture models and guidelines for their use. *J Cereb Blood Flow Metab* 36: 862-890.
75. Weksler BB, Subileau EA, Perriere N, Charneau P, Holloway K, et al. (2005) Blood-brain barrier-specific properties of a human adult brain endothelial cell line. *FASEB J* 19: 1872-1874.
76. Hatherell K, Couraud PO, Romero IA, Weksler B, Pilkington GJ (2011) Development of a three-dimensional, all-human in vitro model of the blood-brain barrier using mono-, co-, and tri-cultivation Transwell models. *J Neurosci Methods* 199: 223-229.
77. Ohtsuki S, Ikeda C, Uchida Y, Sakamoto Y, Miller F, et al. (2013) Quantitative targeted absolute proteomic analysis of transporters, receptors and junction proteins for validation of human cerebral microvascular endothelial cell line hCMEC/D3 as a human blood-brain barrier model. *Mol Pharm* 10: 289-296.
78. Chen H, Winiwarter S, Friden M, Antonsson M, Engkvist O (2011) In silico prediction of unbound brain-to-plasma concentration ratio using machine learning algorithms. *J Mol Graph Model* 29: 985-995.
79. Mahar Doan KM, Humphreys JE, Webster LO, Wring SA, Shampine LJ, et al. (2002) Passive permeability and P-glycoprotein-mediated efflux differentiate central nervous system (CNS) and non-CNS marketed drugs. *J Pharmacol Exp Ther* 303: 1029-1037.
80. Matsson P, Pedersen JM, Norinder U, Bergstrom CA, Artursson P (2009) Identification of novel specific and general inhibitors of the three major human ATP-binding cassette transporters P-gp, BCRP and MRP2 among registered drugs. *Pharm Res* 26: 1816-1831.

81. Norinder U, Haeberlein M (2002) Computational approaches to the prediction of the blood-brain distribution. *Adv Drug Deliv Rev* 54: 291-313.
82. Karlgren M, Simoff I, Backlund M, Wegler C, Keiser M, et al. (2017) A CRISPR-Cas9 Generated Madin-Darby Canine Kidney Expressing Human MDR1 Without Endogenous Canine MDR1 (cABCb1): An Improved Tool for Drug Efflux Studies. *J Pharm Sci*.
83. Simoff I, Karlgren M, Backlund M, Lindstrom AC, Gaugaz FZ, et al. (2016) Complete Knockout of Endogenous Mdr1 (Abcb1) in MDCK Cells by CRISPR-Cas9. *J Pharm Sci* 105: 1017-1021.
84. Loewi O (1957) On the background of the discovery of neurochemical transmission. *J Mt Sinai Hosp N Y* 24: 1014-1016.
85. Oda Y (1999) Choline acetyltransferase: the structure, distribution and pathologic changes in the central nervous system. *Pathol Int* 49: 921-937.
86. Lim SA, Kang UJ, McGehee DS (2014) Striatal cholinergic interneuron regulation and circuit effects. *Front Synaptic Neurosci* 6: 22.
87. Schafer MK, Eiden LE, Weihe E (1998) Cholinergic neurons and terminal fields revealed by immunohistochemistry for the vesicular acetylcholine transporter. I. Central nervous system. *Neuroscience* 84: 331-359.
88. Picciotto MR, Higley MJ, Mineur YS (2012) Acetylcholine as a Neuromodulator: Cholinergic Signaling Shapes Nervous System Function and Behavior. *Neuron* 76: 116-129.
89. Zaborszky L, Csordas A, Mosca K, Kim J, Gielow MR, et al. (2015) Neurons in the Basal Forebrain Project to the Cortex in a Complex Topographic Organization that Reflects Corticocortical Connectivity Patterns: An Experimental Study Based on Retrograde Tracing and 3D Reconstruction. *Cerebral Cortex* 25: 118-137.
90. Everitt BJ, Robbins TW (1997) Central cholinergic systems and cognition. *Annual Review of Psychology* 48: 649-684.
91. Lester DB, Rogers TD, Blaha CD (2010) Acetylcholine-dopamine interactions in the pathophysiology and treatment of CNS disorders. *CNS Neurosci Ther* 16: 137-162.
92. Gielow MR, Zaborszky L (2017) The Input-Output Relationship of the Cholinergic Basal Forebrain. *Cell Reports* 18: 1817-1830.
93. Decker MW (1987) The Effects of Aging on Hippocampal and Cortical Projections of the Forebrain Cholinergic System. *Brain Research Reviews* 12: 423-438.
94. Morikawa H, Paladini CA (2011) Dynamic regulation of midbrain dopamine neuron activity: intrinsic, synaptic, and plasticity mechanisms. *Neuroscience* 198: 95-111.
95. Hirsch E, Graybiel AM, Agid YA (1988) Melanized dopaminergic neurons are differentially susceptible to degeneration in Parkinson's disease. *Nature* 334: 345-348.
96. Le Moal M, Simon H (1991) Mesocorticolimbic dopaminergic network: functional and regulatory roles. *Physiol Rev* 71: 155-234.
97. Bjorklund A, Dunnett SB (2007) Dopamine neuron systems in the brain: an update. *Trends Neurosci* 30: 194-202.
98. Kempadoo KA, Mosharov EV, Choi SJ, Sulzer D, Kandel ER (2016) Dopamine release from the locus coeruleus to the dorsal hippocampus promotes spatial learning and memory. *Proc Natl Acad Sci U S A* 113: 14835-14840.
99. Niederkofler V, Asher TE, Dymecki SM (2015) Functional Interplay between Dopaminergic and Serotonergic Neuronal Systems during Development and Adulthood. *ACS Chem Neurosci* 6: 1055-1070.

100. Schwarz LA, Luo LQ (2015) Organization of the Locus Coeruleus-Norepinephrine System. *Current Biology* 25: R1051-R1056.
101. Dahlstrom A, Fuxe K (1964) Evidence for the Existence of Monoamine-Containing Neurons in the Central Nervous System. I. Demonstration of Monoamines in the Cell Bodies of Brain Stem Neurons. *Acta Physiol Scand Suppl: SUPPL 232*:231-255.
102. Segal M (1979) Serotonergic innervation of the locus coeruleus from the dorsal raphe and its action on responses to noxious stimuli. *J Physiol* 286: 401-415.
103. Wallman MJ, Gagnon D, Parent M (2011) Serotonin innervation of human basal ganglia. *Eur J Neurosci* 33: 1519-1532.
104. Iversen L (2000) Neurotransmitter transporters: fruitful targets for CNS drug discovery. *Mol Psychiatry* 5: 357-362.
105. Kim TH, Choi J, Kim HG, Kim HR (2014) Quantification of neurotransmitters in mouse brain tissue by using liquid chromatography coupled electrospray tandem mass spectrometry. *J Anal Methods Chem* 2014: 506870.
106. Precht W, Yoshida M (1971) Blockage of caudate-evoked inhibition of neurons in the substantia nigra by picrotoxin. *Brain Res* 32: 229-233.
107. Lindsay J, Laurin D, Verreault R, Hebert R, Helliwell B, et al. (2002) Risk factors for Alzheimer's disease: a prospective analysis from the Canadian Study of Health and Aging. *Am J Epidemiol* 156: 445-453.
108. Rodriguez M, Rodriguez-Sabate C, Morales I, Sanchez A, Sabate M (2015) Parkinson's disease as a result of aging. *Aging Cell* 14: 293-308.
109. Mishur RJ, Rea SL (2012) Applications of mass spectrometry to metabolomics and metabonomics: detection of biomarkers of aging and of age-related diseases. *Mass Spectrom Rev* 31: 70-95.
110. Suhara T, Chaki S, Kimura H, Furusawa M, Matsumoto M, et al. (2017) Strategies for Utilizing Neuroimaging Biomarkers in CNS Drug Discovery and Development: CINP/JSNP Working Group Report. *Int J Neuropsychopharmacol* 20: 285-294.
111. Eylers VV, Maudsley AA, Bronzlik P, Dellani PR, Lanfermann H, et al. (2016) Detection of Normal Aging Effects on Human Brain Metabolite Concentrations and Microstructure with Whole-Brain MR Spectroscopic Imaging and Quantitative MR Imaging. *AJNR Am J Neuroradiol* 37: 447-454.
112. Haga KK, Khor YP, Farrall A, Wardlaw JM (2009) A systematic review of brain metabolite changes, measured with 1H magnetic resonance spectroscopy, in healthy aging. *Neurobiol Aging* 30: 353-363.
113. Motyka S, Moser P, Hingerl L, Hangel G, Heckova E, et al. (2019) The influence of spatial resolution on the spectral quality and quantification accuracy of whole-brain MRSI at 1.5T, 3T, 7T, and 9.4T. *Magn Reson Med* 82: 551-565.
114. Grachev ID, Swarnkar A, Szeverenyi NM, Ramachandran TS, Apkarian AV (2001) Aging alters the multichemical networking profile of the human brain: an in vivo (1)H-MRS study of young versus middle-aged subjects. *J Neurochem* 77: 292-303.
115. Mattson MP, Magnus T (2006) Ageing and neuronal vulnerability. *Nat Rev Neurosci* 7: 278-294.
116. Haycock JW, Becker L, Ang L, Furukawa Y, Hornykiewicz O, et al. (2003) Marked disparity between age-related changes in dopamine and other presynaptic dopaminergic markers in human striatum. *Journal of Neurochemistry* 87: 574-585.
117. Ma SY, Ciliax BJ, Stebbins G, Jaffar S, Joyce JN, et al. (1999) Dopamine transporter-immunoreactive neurons decrease with age in the human substantia nigra. *Journal of Comparative Neurology* 409: 25-37.

118. Kaasinen V, Vilkmann H, Hietala J, Nagren K, Helenius H, et al. (2000) Age-related dopamine D2/D3 receptor loss in extrastriatal regions of the human brain. *Neurobiology of Aging* 21: 683-688.
119. Terao A, Steininger TL, Morairty SR, Kilduff TS (2004) Age-related changes in histamine receptor mRNA levels in the mouse brain. *Neuroscience Letters* 355: 81-84.
120. Mazurkiewiczzkwilecki IM, Prell GD (1984) Age-Related-Changes in Brain Histamine. *Agents and Actions* 14: 554-557.
121. Bartus RT, Dean RL, 3rd, Beer B, Lippa AS (1982) The cholinergic hypothesis of geriatric memory dysfunction. *Science* 217: 408-414.
122. Seidler RD, Bernard JA, Burutolu TB, Fling BW, Gordon MT, et al. (2010) Motor control and aging: Links to age-related brain structural, functional, and biochemical effects. *Neuroscience and Biobehavioral Reviews* 34: 721-733.
123. Dreher JC, Meyer-Lindenberg A, Kohn P, Berman KF (2008) Age-related changes in midbrain dopaminergic regulation of the human reward system. *Proceedings of the National Academy of Sciences of the United States of America* 105: 15106-15111.
124. Arnsten AFT (1998) Catecholamine modulation of prefrontal cortical cognitive function. *Trends in Cognitive Sciences* 2: 436-447.
125. Li SC, Lindenberger U, Sikstrom S (2001) Aging cognition: from neuromodulation to representation. *Trends in Cognitive Sciences* 5: 479-486.
126. Mather M, Harley CW (2016) The Locus Coeruleus: Essential for Maintaining Cognitive Function and the Aging Brain. *Trends in Cognitive Sciences* 20: 214-226.
127. Meltzer CC, Smith G, DeKosky ST, Pollock BG, Mathis CA, et al. (1998) Serotonin in aging, late-life depression, and Alzheimer's disease: The emerging role of functional imaging. *Neuropsychopharmacology* 18: 407-430.
128. Yanai K, Watanabe T, Meguro K, Yokoyama H, Sato I, et al. (1992) Age-Dependent Decrease in Histamine H1 Receptor in Human Brains Revealed by Pet. *Neuroreport* 3: 433-436.
129. Paxinos G, Franklin KBJ (2013) Paxinos and Franklin's the mouse brain in stereotaxic coordinates. Amsterdam: Elsevier Academic Press.
130. Abbassi-Ghadi N, Jones EA, Veselkov KA, Huang JZ, Kumar S, et al. (2015) Repeatability and reproducibility of desorption electrospray ionization-mass spectrometry (DESI-MS) for the imaging analysis of human cancer tissue: a gateway for clinical applications. *Analytical Methods* 7: 71-80.
131. Gramatica P (2013) On the development and validation of QSAR models. *Methods Mol Biol* 930: 499-526.
132. Sane R, Agarwal S, Elmquist WF (2012) Brain Distribution and Bioavailability of Elacridar after Different Routes of Administration in the Mouse. *Drug Metabolism and Disposition* 40: 1612-1619.
133. Friden M, Winiwarter S, Jerndal G, Bengtsson O, Wan H, et al. (2009) Structure-Brain Exposure Relationships in Rat and Human Using a Novel Data Set of Unbound Drug Concentrations in Brain Interstitial and Cerebrospinal Fluids. *Journal of Medicinal Chemistry* 52: 6233-6243.
134. Montesinos RN, Moulari B, Gromand J, Beduneau A, Lamprecht A, et al. (2014) Coadministration of P-glycoprotein modulators on loperamide pharmacokinetics and brain distribution. *Drug Metab Dispos* 42: 700-706.
135. Li JB, Wang Y, Hidalgo IJ (2013) Kinetic Analysis of Human and Canine P-Glycoprotein-Mediated Drug Transport in MDR1-MDCK Cell Model: Approaches to Reduce False-Negative Substrate Classification. *Journal of Pharmaceutical Sciences* 102: 3436-3446.

136. Muller L, Baldwin K, Barbacci DC, Jackson SN, Roux A, et al. (2017) Laser Desorption/Ionization Mass Spectrometric Imaging of Endogenous Lipids from Rat Brain Tissue Implanted with Silver Nanoparticles. *J Am Soc Mass Spectrom* 28: 1716-1728.
137. Swales JG, Tucker JW, Spreadborough MJ, Iverson SL, Clench MR, et al. (2015) Mapping Drug Distribution in Brain Tissue Using Liquid Extraction Surface Analysis Mass Spectrometry Imaging. *Analytical Chemistry* 87: 10146-10152.
138. Seneca N, Zoghbi SS, Liow JS, Kreisl W, Herscovitch P, et al. (2009) Human brain imaging and radiation dosimetry of <sup>11</sup>C-N-desmethyl-loperamide, a PET radiotracer to measure the function of P-glycoprotein. *J Nucl Med* 50: 807-813.
139. Englund G, Lundquist P, Skogastierna C, Johansson J, Hoogstraate J, et al. (2014) Cytochrome P450 Inhibitory Properties of Common Efflux Transporter Inhibitors. *Drug Metabolism and Disposition* 42: 441-447.
140. Kim KA, Chung JG, Jung DH, Park JY (2004) Identification of cytochrome P450 isoforms involved in the metabolism of loperamide in human liver microsomes. *European Journal of Clinical Pharmacology* 60: 575-581.
141. Yoshimoto K, Echizen H, Chiba K, Tani M, Ishizaki T (1995) Identification of human CYP isoforms involved in the metabolism of propranolol enantiomers--N-desisopropylation is mediated mainly by CYP1A2. *Br J Clin Pharmacol* 39: 421-431.
142. Bankstahl JP, Bankstahl M, Romermann K, Wanek T, Stanek J, et al. (2013) Tariquidar and Elacridar Are Dose-Dependently Transported by P-Glycoprotein and Bcrp at the Blood-Brain Barrier: A Small-Animal Positron Emission Tomography and In Vitro Study. *Drug Metabolism and Disposition* 41: 754-762.
143. Hampel H, Mesulam MM, Cuello AC, Farlow MR, Giacobini E, et al. (2018) The cholinergic system in the pathophysiology and treatment of Alzheimer's disease. *Brain* 141: 1917-1933.
144. Birks J (2006) Cholinesterase inhibitors for Alzheimer's disease. *Cochrane Database of Systematic Reviews*.
145. Blokland A (1995) Acetylcholine: a neurotransmitter for learning and memory? *Brain Res Brain Res Rev* 21: 285-300.
146. Euston DR, Gruber AJ, McNaughton BL (2012) The role of medial prefrontal cortex in memory and decision making. *Neuron* 76: 1057-1070.
147. Anzalone S, Roland J, Vogt B, Savage L (2009) Acetylcholine efflux from retrosplenial areas and hippocampal sectors during maze exploration. *Behav Brain Res* 201: 272-278.
148. Gage SL, Keim SR, Simon JR, Low WC (1994) Cholinergic innervation of the retrosplenial cortex via the fornix pathway as determined by high affinity choline uptake, choline acetyltransferase activity, and muscarinic receptor binding in the rat. *Neurochem Res* 19: 1379-1386.
149. Nestor PJ, Fryer TD, Ikeda M, Hodges JR (2003) Retrosplenial cortex (BA 29/30) hypometabolism in mild cognitive impairment (prodromal Alzheimer's disease). *Eur J Neurosci* 18: 2663-2667.
150. Pengas G, Hodges JR, Watson P, Nestor PJ (2010) Focal posterior cingulate atrophy in incipient Alzheimer's disease. *Neurobiol Aging* 31: 25-33.
151. Pengas G, Williams GB, Acosta-Cabrero J, Ash TW, Hong YT, et al. (2012) The relationship of topographical memory performance to regional neurodegeneration in Alzheimer's disease. *Front Aging Neurosci* 4: 17.
152. Tan RH, Wong S, Hodges JR, Halliday GM, Hornberger M (2013) Retrosplenial cortex (BA 29) volumes in behavioral variant frontotemporal dementia and Alzheimer's disease. *Dement Geriatr Cogn Disord* 35: 177-182.

153. Schliebs R, Arendt T (2006) The significance of the cholinergic system in the brain during aging and in Alzheimer's disease. *Journal of Neural Transmission* 113: 1625-1644.
154. Schliebs R, Arendt T (2011) The cholinergic system in aging and neuronal degeneration. *Behavioural Brain Research* 221: 555-563.
155. Summerfield SG, Zhang Y, Liu H (2016) Examining the Uptake of Central Nervous System Drugs and Candidates across the Blood-Brain Barrier. *J Pharmacol Exp Ther* 358: 294-305.
156. Telting-Diaz M, Lunte CE (1993) Distribution of tacrine across the blood-brain barrier in awake, freely moving rats using in vivo microdialysis sampling. *Pharm Res* 10: 44-48.
157. Gao HY, Deng SB, Obach RS (2010) A Simple Liquid Chromatography-Tandem Mass Spectrometry Method to Determine Relative Plasma Exposures of Drug Metabolites across Species for Metabolite Safety Assessments. *Drug Metabolism and Disposition* 38: 2147-2156.
158. McNally WP, Pool WF, Sinz MW, Dehart P, Ortwine DF, et al. (1996) Distribution of tacrine and metabolites in rat brain and plasma after single- and multiple-dose regimens - Evidence for accumulation of tacrine in brain tissue. *Drug Metabolism and Disposition* 24: 628-633.
159. Kinirons MT, O'Mahony MS (2004) Drug metabolism and ageing. *Br J Clin Pharmacol* 57: 540-544.
160. Knight LS, Piibe Q, Lambie I, Perkins C, Yancey PH (2017) Betaine in the Brain: Characterization of Betaine Uptake, its Influence on Other Osmolytes and its Potential Role in Neuroprotection from Osmotic Stress. *Neurochem Res* 42: 3490-3503.
161. White HL, Scates PW (1990) Acetyl-L-carnitine as a precursor of acetylcholine. *Neurochem Res* 15: 597-601.
162. Lee NY, Choi HO, Kang YS (2012) The acetylcholinesterase inhibitors competitively inhibited an acetyl L-carnitine transport through the blood-brain barrier. *Neurochem Res* 37: 1499-1507.
163. Sung JH, Yu KH, Park JS, Tsuruo T, Kim DD, et al. (2005) Saturable distribution of tacrine into the striatal extracellular fluid of the rat: evidence of involvement of multiple organic cation transporters in the transport. *Drug Metab Dispos* 33: 440-448.
164. Binienda ZK (2003) Neuroprotective effects of L-carnitine in induced mitochondrial dysfunction. *Ann N Y Acad Sci* 993: 289-295; discussion 345-289.
165. Imperato A, Ramacci MT, Angelucci L (1989) Acetyl-L-carnitine enhances acetylcholine release in the striatum and hippocampus of awake freely moving rats. *Neurosci Lett* 107: 251-255.
166. Jones LL, McDonald DA, Borum PR (2010) Acylcarnitines: role in brain. *Prog Lipid Res* 49: 61-75.
167. Rizzo AM, Berselli P, Zava S, Montorfano G, Negroni M, et al. (2010) Endogenous antioxidants and radical scavengers. *Adv Exp Med Biol* 698: 52-67.
168. Shigenaga MK, Hagen TM, Ames BN (1994) Oxidative damage and mitochondrial decay in aging. *Proc Natl Acad Sci U S A* 91: 10771-10778.
169. Boldyrev AA, Aldini G, Derave W (2013) Physiology and pathophysiology of carnosine. *Physiol Rev* 93: 1803-1845.
170. Hipkiss AR, Baye E, de Courten B (2016) Carnosine and the processes of ageing. *Maturitas* 93: 28-33.
171. Serbinova E, Kagan V, Han D, Packer L (1991) Free radical recycling and intramembrane mobility in the antioxidant properties of alpha-tocopherol and alpha-tocotrienol. *Free Radic Biol Med* 10: 263-275.

172. Cutler RG, Kelly J, Storie K, Pedersen WA, Tammara A, et al. (2004) Involvement of oxidative stress-induced abnormalities in ceramide and cholesterol metabolism in brain aging and Alzheimer's disease. *Proc Natl Acad Sci U S A* 101: 2070-2075.
173. Kim M, Nevado-Holgado A, Whiley L, Snowden SG, Soininen H, et al. (2017) Association between Plasma Ceramides and Phosphatidylcholines and Hippocampal Brain Volume in Late Onset Alzheimer's Disease. *J Alzheimers Dis* 60: 809-817.
174. Hernandez-Corbacho MJ, Jenkins RW, Clarke CJ, Hannun YA, Obeid LM, et al. (2011) Accumulation of long-chain glycosphingolipids during aging is prevented by caloric restriction. *PLoS One* 6: e20411.
175. Vozella V, Basit A, Misto A, Piomelli D (2017) Age-dependent changes in nervonic acid-containing sphingolipids in mouse hippocampus. *Biochim Biophys Acta Mol Cell Biol Lipids* 1862: 1502-1511.
176. Westerink BHC (1985) Sequence and Significance of Dopamine Metabolism in the Rat-Brain. *Neurochemistry International* 7: 221-227.
177. Fowler CJ, Wiberg A, Orelund L, Marcusson J, Winblad B (1980) The Effect of Age on the Activity and Molecular-Properties of Human-Brain Monoamine-Oxidase. *Journal of Neural Transmission* 49: 1-20.
178. Eisenhofer G, Kopin IJ, Goldstein DS (2004) Catecholamine metabolism: A contemporary view with implications for physiology and medicine. *Pharmacological Reviews* 56: 331-349.
179. Ohtsuki S, Asaba H, Takanaga H, Deguchi T, Hosoya K, et al. (2002) Role of blood-brain barrier organic anion transporter 3 (OAT3) in the efflux of indoxyl sulfate, a uremic toxin: its involvement in neurotransmitter metabolite clearance from the brain. *Journal of Neurochemistry* 83: 57-66.
180. Jacobs BL, Azmitia EC (1992) Structure and Function of the Brain-Serotonin System. *Physiological Reviews* 72: 165-229.
181. Haas HL, Sergeeva OA, Selbach O (2008) Histamine in the nervous system. *Physiological Reviews* 88: 1183-1241.
182. Cumming P, Reiner PB, Vincent SR (1990) Inhibition of Rat-Brain Histamine-N-Methyltransferase by 9-Amino-1,2,3,4-Tetrahydroacridine (Tha). *Biochemical Pharmacology* 40: 1345-1350.
183. Anden NE, Carlsson A, Dahlstrom A, Fuxe K, Hillarp NA, et al. (1964) Demonstration and Mapping out of Nigro-Neostriatal Dopamine Neurons. *Life Sciences* 3: 523-530.
184. Yassa MA, Mattfeld AT, Stark SM, Stark CE (2011) Age-related memory deficits linked to circuit-specific disruptions in the hippocampus. *Proc Natl Acad Sci U S A* 108: 8873-8878.



# Acta Universitatis Upsaliensis

*Digital Comprehensive Summaries of Uppsala Dissertations  
from the Faculty of Pharmacy 278*

Editor: The Dean of the Faculty of Pharmacy

A doctoral dissertation from the Faculty of Pharmacy, Uppsala University, is usually a summary of a number of papers. A few copies of the complete dissertation are kept at major Swedish research libraries, while the summary alone is distributed internationally through the series Digital Comprehensive Summaries of Uppsala Dissertations from the Faculty of Pharmacy. (Prior to January, 2005, the series was published under the title "Comprehensive Summaries of Uppsala Dissertations from the Faculty of Pharmacy".)

Distribution: [publications.uu.se](http://publications.uu.se)  
urn:nbn:se:uu:diva-392320



ACTA  
UNIVERSITATIS  
UPSALIENSIS  
UPPSALA  
2019